J.-S. Ardaens, G.V.M. Gaias
Angles-Only Relative Orbit Determination in Low Earth Orbit
Advances in Space Research, Vol. 61, N. 11, 2018, p. 2740-2760
doi:10.1016/j.asr.2018.03.016

Angles-Only Relative Orbit Determination in Low Earth Orbit

Jean-Sébastien Ardaens[1], Gabriella Gaias

DLR, German Aerospace Center, 82234 Wessling, Germany

Abstract

The paper provides an overview of the angles-only relative orbit determination activities conducted to support the Autonomous Vision Approach Navigation and Target Identification (AVANTI) experiment. This in-orbit endeavor was carried out by the German Space Operations Center (DLR/GSOC) in autumn 2016 to demonstrate the capability to perform spaceborne autonomous close-proximity operations using solely line-of-sight measurements. The images collected onboard have been reprocessed by an independent on-ground facility for precise relative orbit determination, which served as ultimate instance to monitor the formation safety and to characterize the onboard navigation and control performances. During two months, several rendezvous have been executed, generating a valuable collection of images taken at distances ranging from 50 km to only 50 m. Despite challenging experimental conditions characterized by a poor visibility and strong orbit perturbations, angles-only relative positioning products could be continuously derived throughout the whole experiment timeline, promising accuracy at the meter level during the close approaches. The results presented in the paper are complemented with former angles-only experience gained with the PRISMA satellites to better highlight the specificities induced by different orbits and satellite designs.

Keywords: angles-only navigation; noncooperative rendezvous; formation-flying; flight demonstration

Email address: jean-sebastien.ardaens@dlr.de (Jean-Sébastien Ardaens)
[1]Corresponding author.

1. Introduction

Rendezvous with a noncooperative target is a key technological capability for many space activities, including on-orbit servicing, active debris removal, sample return or even asteroid exploration. A target is qualified as noncooperative when it does not foresee any kind of cooperation with the chaser satellite, either because it has become inactive or because it was not designed to ease any rendezvous. In this case, safely navigating to such an object becomes a real challenge, so that a safe and reliable approach is often guaranteed at the expense of costly additional sensors and ground support.

It has been early recognized that passive imagery could play a predominant role in the sensor assembly required for the relative navigation (Fehse, 2003; Cropp, 2001). A camera is a simple, cheap, small, light-weight and low-power consumption device presenting a high readiness level. This makes it perfectly suited to support the navigation task, delivering line-of-sight measurements at far-range when the shape of the target cannot be distinguished and allowing advanced shape-matching techniques at close-range. This appealing sensing capability comes however at the cost of a very weak observability (in case of line-of-sight navigation) and a dependency to lightening conditions. In other words, the simplicity of the sensor is counterbalanced afterwards by advanced processing techniques to extract reliably the measurements from the picture and estimate accurately the relative motion despite the weak observability and the measurement outages.

The work presented in the paper focuses on the far to mid-range domain, where only line-of-sight observations are accessible. The problem of angles-only (or bearings-only) navigation is not new and has been already extensively addressed in the literature. In fact, this technique has been already used for instance in naval applications (Nardone and Graham, 1997) or for orbit determination (Sabol and Vallado, 1999) of satellites. More recently, it has been recognized that angles-only measurements might as well help navigating in space. Chari (2001) and Woffinden (2008) have both provided major contributions to this field by investigating the usage of angles-only navigation for autonomous orbital rendezvous. Among the research topics, the problem of observability has attracted considerable attention (Nardone and Aidala, 1981; Hammel and Aidala, 1985; Woffinden and Geller, 2009; Yim et al., 2004), and especially the quest for maneuvers which best contribute to improve the observability or relative trajectories providing better navigation performance (Grzymisch and Fichter, 2015). More recently, the

problem of angles-only navigation even in the absence of maneuvers was also investigated (Sullivan and D'Amico, 2017).

Overall the research areas remained rather theoretical. Numerical simulations were sometimes used to support the investigations, but no author could afford building a testbed in space for realistic performance analysis. In real conditions, the angles-only relative navigation problem becomes more arduous. First, because of the perturbations of the relative motion which can hardly be simulated with high fidelity (for example the differential drag or maneuver execution errors). The distribution over time and the errors affecting the measurements are also extremely difficult to be faithfully modelled (they depend on the orbit and on the target object). Finally, all the authors take for granted the availability of a set of bearing observations. In reality, the extraction of the measurements from the images is sometimes not obvious. The simulations are thus often too limited to assess realistically the achievable performance and the robustness of the line-of-sight navigation.

It is generally admitted that the first relevant experience with angles-only relative navigation in orbit has been collected in 2007 in the frame of Orbital Express, a technology demonstration mission for on-orbit servicing from the American Defense Advanced Research Projects Agency (Orb, 2007). Among the different activities conducted during the mission lifetime, a noncooperative autonomous approach based mainly on passive imagery has been conducted. However the outcome of the mission remained rather confidential, making difficult to assess what has been precisely done and achieved. The Prototype Research Instruments and Space Mission Technology Advancement (PRISMA) formation-flying demonstrator (Persson et al., 2005) constituted the second major gain of flight experience. Among others, it offered the possibility to image a target satellite using a dedicated Vision-Based Sensor (VBS) composed of two different cameras (far- and close-range). Thanks to a dedicated program located in its data processing unit, the far-range sensor was able to extract line-of-sight measurements of the luminous objects which were not included in its star catalog. Several vision-based rendezvous activities have been conducted by the different partners of the mission. The Autonomous Rendezvous experiment (ARV) led by the former Swedish Space Corporation could exercise angles-only navigation using the line-of-sight observations delivered in real-time by the VBS (Noteborn et al., 2011). The French and German space agencies (respectively CNES and DLR) performed their own investigations on angles-only navigation. The CNES experiment relied as well on the measurements extracted by the sensor (Delpech et al.,

2012). The DLR activities were instead designed to work directly with the pictures output by the camera and culminated with the ARGON (Advanced Rendezvous demonstration using GPS and Optical Navigation) experiment (D'Amico et al., 2013), which demonstrated the ability to perform a ground-in-loop approach from 30 km to 3 km to a noncooperative target using solely line-of-sight measurements.

The fruitful experience gained with the PRISMA satellites served as baseline to design and implement the more complex AVANTI (Autonomous Vision Approach Navigation and Target Identification) experiment (Gaias et al., 2017). This technological demonstration was conducted in autumn 2016 and could successfully show in orbit the ability to *fully autonomously* approach a passive object in a safe and fuel-efficient way using only line-of-sight measurements provided by a single camera. A dedicated standalone spaceborne application had been designed to reach this ambitious goal, requiring the development of novel complex algorithms to autonomously handle the attitude profile of the satellite, to acquire and process images in real-time, detect the target spacecraft and derive a relative state estimate, and finally to compute and execute maneuvers according to a guidance plan satisfying numerous constraints. It has to be emphasized that, contrary to all experiments done with the PRISMA satellites, AVANTI has been conceived to deal with a truly uncooperative target, relying only on pictures to estimate precisely the state of the formation and to guarantee its safety. In view of the complexity and experimental status of the onboard software, it appeared early obvious that a ground-based verification layer would be needed to support the characterization and validation of the onboard algorithms, giving the birth to the ground facility for precise vision-based relative orbit determination. Compared to the onboard real-time navigation, the ground-based orbit determination benefits from larger computational power (allowing thus for more advanced and accurate algorithms) and from the critical eye of the human operator, able to better assess the plausibility of the solution. As a consequence, the resulting reconstructed relative trajectory becomes the best possible post-facto knowledge of the state of the formation, which can serve as reference to characterize the performance of the onboard algorithms and of course as ultimate instance to monitor the safety of the formation during the close approaches.

During ARGON, frequent angles-only relative orbit determinations had to be performed to support the rendezvous. For this purpose, a dedicated batch least-squares filter had been developed to estimate the relative motion based

on relative orbital elements (Gaias et al., 2014), providing a first valuable assessment of the achievable relative navigation performance in real conditions (D'Amico et al., 2013). The precise orbit determination for AVANTI relies on this heritage and has been improved to cope with the much more demanding experimental conditions: strong orbit perturbations and poor visibility conditions resulting in very sparse measurements.

The paper aims at providing a comprehensive overview of the angles-only relative orbit determination done to support the AVANTI mission. The first section describes the experimental conditions more in details and highlights the specificities of AVANTI. The second section provides a description of the relative orbit determination task. The largest part is dedicated to the target detection and represents one of the main contributions of this work: how to deliver reliable observations to the relative navigation filter. To the knowledge of the authors, this aspect has not been investigated deeply in the literature. The built-in target detection software (Benn and Jørgensen, 2013) of the VBS constitutes one of the few available references. Being implemented directly in the camera system, the algorithm is able to run at high frequency (2 Hz) and detects non-stellar objects based on their expected inertial angular velocity. The sensor keeps track internally of all the detected objects and delivers only the best candidate, based on the luminosity and the number of sequential detections. During the PRISMA operations, some false detections were however sometimes reported (Noteborn et al., 2011; Delpech et al., 2012). In addition, this strategy appears more difficult to implement considering the low image rate used during AVANTI (one image every 30 seconds). During the ARGON experiment, a target detection algorithm based on linking bright connected sets of pixels over sequences of images had been used (Benninghoff et al., 2013). However, the algorithm was also subject to some misdetections (D'Amico et al., 2013). For AVANTI, a novel algorithm has been developed, based on the kinematic detection of target trajectories. The underlying idea is that the target object obeys as well the law of space dynamics, so that its apparent trajectories can be recognized as a curve, conferring additional robustness to the detection algorithm. In addition, the algorithm exploits in a second step its proximity to the relative orbit determination task to further filter out the possible outliers.

Finally the paper presents the flight results obtained during the AVANTI campaign, which constitutes the second major contribution of the paper. It has been found fruitful to complement the discussions with some additional results from ARGON, whose data have been reprocessed in the same way

to better highlight the effects induced by fairly different experimental conditions. The section covers the initial target acquisition at 50 km distance up to the closest approach at about 50 m distance, and describes the experience gained in terms of target visibility and detection, influence of orbit perturbations, and relative orbit determination performance.

2. Experimental Framework

2.1. The ARGON Heritage

As already mentioned previously, the ARGON experiment has been conducted in April 2012 using the PRISMA satellites, launched in 2010 in a Sun-synchronous dawn-dusk orbit at about 750 km altitude and composed of two small spacecraft (cf. Fig. 1): Mango, equipped with a propulsion system and bedecked with different formation-flying sensors, following actively Tango, a more simple satellite. During the mission timeline, numerous advanced formation-flying activities were conducted (Bodin et al., 2012), among which the 5-day-long ARGON experiment, aiming at demonstrating the ability to conduct a ground-in-the-loop vision-based rendezvous to a noncooperative target. Mango played the role of the chaser spacecraft in charge of the approach. Tango, which had been considered as noncooperative for the sake of the experiment, took the role of the target. This

Figure 1: The PRISMA formation: Mango (left) chasing Tango (right) (image credit: OHB-Sweden).

on-orbit demonstration could benefit from the technological wealth offered by a formation-flying testbed: 3D maneuver capability, precise attitude control and dedicated far-range tracking camera on the chaser side. Both spacecraft were in addition equipped with a GPS receiver for precise real-time relative navigation (D'Amico et al., 2006). This feature was not directly used during

Items	Value	Unit
Field of view	18.3 x 13.7	deg
Resolution	752 x 580	pixel
Focal Length	20	mm

(a) Camera Parameters.

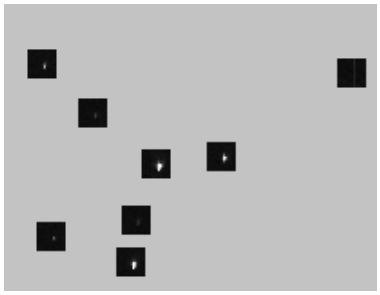

(b) Delivery of Regions of Interests.

Figure 2: Some relevant characteristics of the μASC star tracker.

the experiment but was in the background always active for formation safety monitoring, so that valuable accurate measurements of the formation at any time could be stored for further investigations. The existence of precise relative positioning products derived *post-facto* using the raw (code and carrier phase) GPS data (Ardaens et al., 2011) constitutes in fact a precious asset for the precise analysis of the navigation and control errors, but also for the characterization of the sensor and image processing performance.

The VBS far-range sensor used to track the target object was a modified version on the fully autonomous miniaturized μASC star-tracker (Jørgensen et al., 2003), whose main characteristics are summarized in Table 2a. The same sensor would be later used for AVANTI, allowing for extensive transfer of experience between both experiments. As already explained in the introduction, with respect to the traditional star-tracker the VBS introduces an electronic shutter control for improved dynamic range and dedicated algorithms located in the digital processing unit to detect automatically non-stellar objects (Jørgensen and Benn, 2010). During ARGON, it has been preferred to directly process the raw images, so that this second feature has in fact never been used.

In order to cope with the limited data budget of the satellite, a special feature of the camera allowed sending only most important information of the image, by automatically selecting a Region of Interest (16x16 pixels) around the luminous objects detected in the image as depicted in Fig. 2b. This feature made a large reduction of the size of the image possible, but introduced some limitations when the distance decreased, since the target object did not fit anymore into the small area allocated to the Region of

Interest, introducing massive centroiding errors (D'Amico et al., 2013).

2.2. The AVANTI Contribution

The AVANTI experiment has been conducted in autumn 2016 and aimed at demonstrating spaceborne vision-based autonomous approach to a non-cooperative target. AVANTI has been implemented as passenger software onboard the DLR's BIROS satellite (Halle et al., 2014), which is primarily an Earth-observation satellite whose orbit is chosen to be close to the Earth's surface (515 km altitude, local time of ascending node 21:30). The choice of BIROS as chaser for this in-orbit demonstration was not mere coincidence: the satellite embarked in fact a third-party picosatellite (named BEESAT-4 (Baumann et al., 2012)) which was released in-orbit by the means of a picosatellite launcher (Roemer and Stoltz, 2010) and could thus serve as noncooperative target for the sake of the experiment (cf. Fig. 3), without the need of spending a large amount of propellant to navigate to an existing space debris. The major advance of the experiment is summarized in the first letter of the name: *autonomy*. Since all tasks had to be executed onboard, the core algorithms have been implemented as additional guidance navigation and control (GNC) modes directly interfaced to the Attitude and Orbit Control System (AOCS) of the chaser spacecraft (Gaias et al., 2017), implying that the onboard AVANTI software module had full translational and rotational control of the chaser satellite during the experiment lifetime.

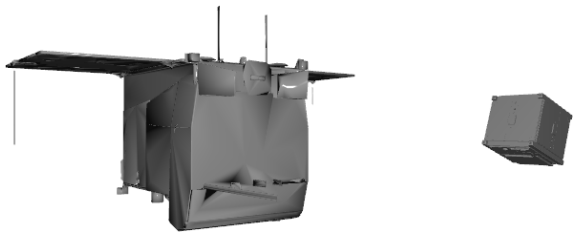

Figure 3: The AVANTI formation: BIROS (left) chasing BEESAT-4 (right).

This peculiar experimental framework induced some additional difficulties, which make the Authors believe that AVANTI represents a sort of worst case scenario in terms of angles-only rendezvous in orbit (Gaias et al., 2015). Contrary to the ARGON experiment which, thanks to the dawn-dusk orbit of the PRISMA satellites, benefited from optimal illumination conditions, AVANTI is meant for approaching target objects flying on any kind of low

Earth orbits. As depicted in Fig. 4, this has dramatic impacts in terms of visibility, since the target object is eclipsed during a large part of the orbit (black part of the relative elliptical motion) and the camera becomes blinded by the Sun during another large part of the orbit (represented in gray). As shown in the figure, the camera is blinded during a large period of time. This is due to the fact that, at far-range, the exposure time of the camera is set to a high value (0.25 s) in order to track the faint objects (up to a visual magnitude of 6-7). Even if the camera is not directly pointing to the Sun, multiple reflections of light within its baffle might be enough to blind it. A Sun-exclusion angle of 70°(according to the constructor) has thus to be kept in far-range mode to ensure the proper functioning of the camera.. As a result, only a tiny portion of the relative motion can be observed, weakening thus the observability property.

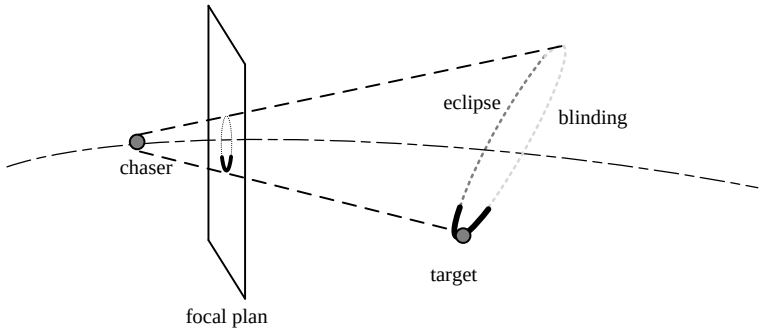

Figure 4: Limited visible relative motion in low Earth orbits. The part of the trajectory which is not visible is represesented by a dashed line.

The second major difference with respect to ARGON is due to the low altitude of the BIROS orbit. Combined with the fact that BIROS and BEESAT-4 differ greatly in shape and mass, featuring thus a very different ballistic coefficient, this induces a strong unknown differential drag which has to be estimated as part of the relative navigation process.

The third difference comes with the limited onboard resources and the constraints posed by the satellite. In particular, it had been chosen to make use of one of the existing star cameras to follow the picosatellite instead of using a dedicated tracking camera like in PRISMA, resulting in a non-nominal attitude profile which in turns conflicted with the power and thermal requirements. As a result, dedicated phases were necessary to cool down the satellite during which the target was not anymore in the field of view. Furthermore,

BIROS was equipped with a single-direction thruster, so that dedicated slews of the satellites were necessary to execute maneuvers, reducing further the time allotted to observe the target. Last but not least, the frequency of observations was limited to one image every 30 seconds to cope with the limited data bandwidth of the onboard computer. As highlighted in the sequel, all these constraints contributed to a very limited amount of measurements.

The final major difficulty of AVANTI lies in the lack of any external reference for cross-validation. Contrary to ARGON, no differential GPS could support the experiment, making the monitoring of the formation safety much more difficult and the subsequent analysis of the system performance. As already explained, the results of the precise orbit determination done on ground are the best possible post-facto knowledge of the state of the formation. This optimistic statement should not lead us to overlook that in such conditions (degraded visibility conditions and strong orbit perturbations), angles-only relative orbit determination in low Earth orbit remains a delicate task. As a result, collecting valuable in-orbit experience regarding the system behavior and the achievable performance was also part of the experiment. In order to obtain a unique independent assessment of the accuracy of the relative trajectory reconstruction, a short ground-based radar tracking campaign has been carried out during the commissioning of AVANTI using the German TIRA (Tracking and Imaging Radar) ground station of the Fraunhofer-Institut für Hochfrequenzphysik und Radartechnik.

2.3. The AVANTI campaign

Two months in orbit were necessary for the successful completion of the experiment, most of the time being dedicated to a thorough commissioning of the spacecraft. Dealing with spaceborne autonomous close-proximity formation-flight, it was indeed necessary to ensure that all subsystems involved in the experiment were working properly before starting an autonomous approach. As depicted in Fig. 5, following the ejection of BEESAT-4 on 9 September 2016, several rendezvous and recedes with different levels of autonomy could be already exercised during the commissioning phase, generating a valuable collection of images at different ranges. Once the satellite was commissioned, the full featured experiment could start on 19 November 2016, during which two autonomous approaches were performed, first from 13 km to 1 km, then from 3 km to 50 m (Gaias et al., 2017).

The problem of angles-only navigation presents different flavors depending on the intersatellite distance. Since AVANTI covered the full range between

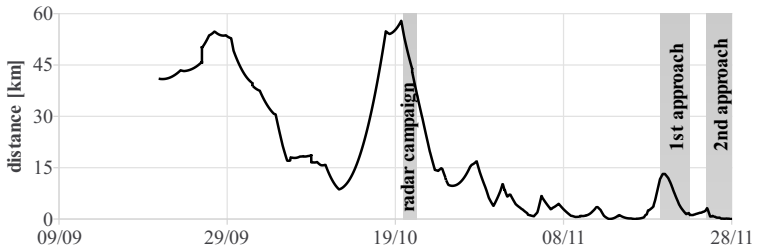

Figure 5: Intersatellite distance during the AVANTI campaign.

50 km to 50 m, the following scenarios could be investigated during the experiment:

- **First acquisition**. This corresponds to the first contact with the target object at far-range, typically several dozen kilometers. The main difficulty here is to be able to distinguish the target and to perform a meaningful orbit determination given the hardly observable variations of relative motion at this distance.

- **Far to mid-range approach**. This range covers the main objective of the AVANTI experiment, namely the ability to autonomously navigate towards a desired hold point at a few hundred meters distance, far enough to guarantee homogenous visibility and brightness conditions throughout the entire approach.

- **Towards close-range**. When decreasing further the distance, the increasing brightness and target size degrade greatly the accuracy of the line-of-sight measurements, posing new challenges to the relative navigation.

The peculiarities encountered at different distances will be described more in details in Section 4.

2.4. Enforcing the Formation Safety

The safety considerations play a major role when dealing with experiments conducted in orbits. In particular, it has to be ensured that, even in the presence of navigation errors, the formation remains safe at any time. These investigations are facilitated by the introduction of a dedicated formation-flying toolset, recalled quickly here to ease the discussions done in the sequel. The relative motion is described using a special parameterization, described

by a set $\delta\boldsymbol{\alpha}$ of dimensionless Relative Orbital Elements (or ROEs, the Reader is invited to refer to Reference Gaias et al. (2014) for more details):

$$\delta\boldsymbol{\alpha} = \begin{pmatrix} \delta a & \delta e_x & \delta e_y & \delta i_x & \delta i_y & \delta\lambda \end{pmatrix}^T, \tag{1}$$

where δa is the relative semi-major axis, $\delta\boldsymbol{e} = \begin{pmatrix} \delta e_x, \delta e_y \end{pmatrix}^T$ and $\delta\boldsymbol{i} = \begin{pmatrix} \delta i_x, \delta i_y \end{pmatrix}^T$ are called respectively relative eccentricity and inclination vectors, and $\delta\lambda$ stands for the relative mean longitude. The relative orbital elements are used to describe the state of the formation and can, if needed, easily be translated into a Cartesian representation. Fig. 6 depicts for example the relative motion in a local Cartesian orbital frame (Radial-Tangential-Normal or R-T-N), whose unit vectors are defined using the satellite position $\hat{\boldsymbol{r}}$ and velocity $\hat{\boldsymbol{v}}$ as follows:

$$\boldsymbol{e}_{\mathrm{R}} = \frac{\hat{\boldsymbol{r}}}{\|\hat{\boldsymbol{r}}\|}, \boldsymbol{e}_{\mathrm{N}} = \frac{\hat{\boldsymbol{r}} \times \hat{\boldsymbol{v}}}{\|\hat{\boldsymbol{r}} \times \hat{\boldsymbol{v}}\|}, \boldsymbol{e}_{\mathrm{T}} = \boldsymbol{e}_{\mathrm{N}} \times \boldsymbol{e}_{\mathrm{R}} \tag{2}$$

Fig. 6 shows that the in-plane relative motion (RT plane on the upper right) is described by δa, $\delta\boldsymbol{e}$ and $\delta\lambda$ whereas $\delta\boldsymbol{i}$ is responsible for the cross-track motion (RN plane on the upper left). As already emphasized in the literature (Montenbruck et al., 2006), this parametrization is of great interest when dealing with formation of satellites, since it offers a quick insight into the geometry of the relative motion and a simple criteria to guarantee the safety of the formation. In fact, using a proper phasing of the relative eccentricity and inclination vectors (parallel or anti-parallel configuration) and under the assumption of a small relative semi-major axis δa, it can be ensured that the intersatellite distance in the plane perpendicular to the flight direction (RN plane) will never drop below a certain value d_{m} which depends on δa, $\delta\boldsymbol{e}$ and $\delta\boldsymbol{i}$. This allows the design of relative orbits which are passively safe. By introducing a nonzero relative semi-major axis, a spiraling approach is created that guarantees that the formation will stay safe even in the presence of unexpected events (failure of the thruster system for example). Note that some care has to be taken during the drifting phase if δa is large, since this can lead to a dramatic reduction of d_{m} (Gaias and Ardaens, 2016).

The convenience of this formulation becomes obvious when considering the strong anisotropy exhibited by angles-only navigation: because of the absence of range measurements, the achievable lateral accuracy (that is, perpendicular to the line-of-sight) is always much better than the longitudinal accuracy. In terms of relative orbital elements, this means simply that (at

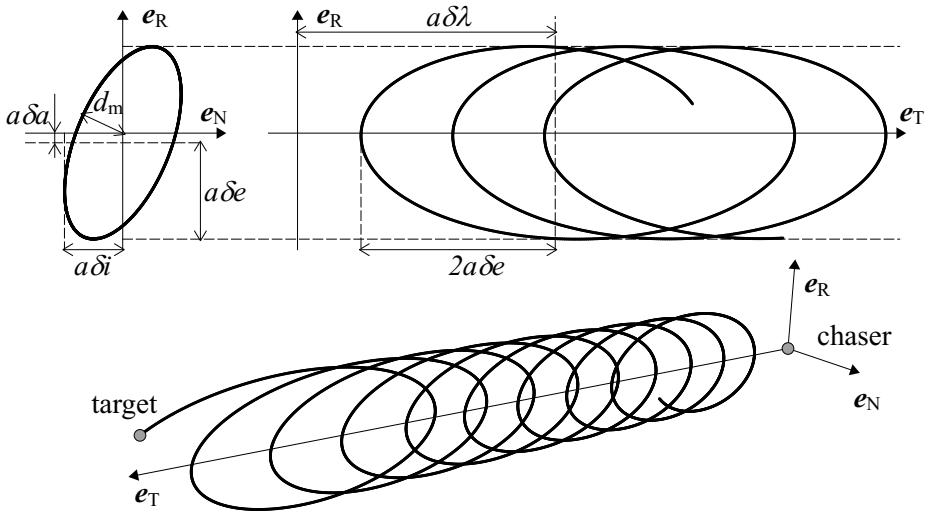

Figure 6: Relative motion parameterized with relative eccentricity/inclination vectors.

far- to mid-range) $\delta\lambda$ is less observable and its estimation will be affected by larger errors, while δa, $\delta\boldsymbol{e}$ and $\delta\boldsymbol{i}$ will be estimated much more accurately, which is exactly what is needed to assess the safety of the formation. Note that this statement applies only to the type of formations considered for a rendezvous, where the along-track component of the relative motion is predominant. In view of their undeniable advantage in terms of formation safety, spiraling approaches has been adopted for both ARGON and AVANTI experiments.

3. Angles-Only Relative Orbit Determination

3.1. Overview

As already mentioned, the apparent simplicity offered by passive imagery comes at the cost of additional processing difficulties. Before making use of line-of-sight measurements, it is first necessary to extract them from the pictures. This is the task of the target identification module (cf. Fig. 7), which is in charge of providing a set of observations to the relative orbit determination.

This precise estimation of the relative trajectory is done a posteriori on ground and is thus subject to very few restrictions concerning the computational and data storage resources. As a result, in view of the sparse ob-

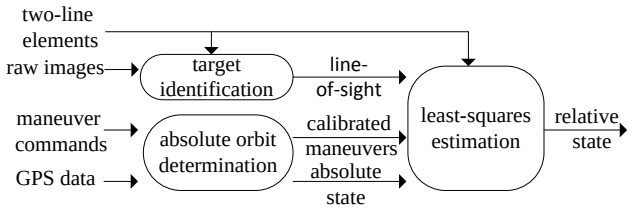

Figure 7: Functional view of the overall relative orbit determination task.

servations and the weak observability of the problem, a batch least-squares approach is preferred to improve the overall robustness of the solution. By considering long observations arcs, it is indeed possible to observe the long-term effects of perturbations (for instance the differential drag) which are otherwise difficult to be estimated properly. Furthermore, the resulting iterative refinement of the solution is well adapted to remove the possible outliers of the observations which could degrade the accuracy. The least-squares adjustment is facilitated using a reference solution, around which the quantities are linearized. It has been chosen to make use of a two-line element (TLE) set to derive an approximate value of the state, which can easily be justified by the fact that almost all orbiting objects larger than 10 cm are catalogized as part of the space awareness activities, so that any rendezvous in low Earth orbit with a noncooperative satellite can rely on TLEs for initial target acquisition. Moreover, as described later in the paper, the TLEs appear to be the ideal companion for angles-only navigation at far range: while the latter is extremely precise in lateral positioning, but has trouble estimating properly the intersatellite separation, the former provides a valuable estimate of the relative distance. The position error of the two-line elements amounts typically to hundreds of meters (or even a few kilometers), which corresponds only to a few percent of error when starting the approach at 50 km distance.

In the adopted design, the least-squares method tries to adjust a numerically propagated relative trajectory to best fit the available line-of-sight measurements. In order to improve the observability, it is sufficient to execute maneuvers altering the relative motion (Woffinden and Geller, 2009), which is fortunately the case during a rendezvous. In order to reduce the errors of the dynamical model, the maneuvers executed by the chaser are calibrated prior to the relative orbit determination. This calibration is done using GPS data collected onboard as part of a GPS-based orbit determination combining code and low-noise carrier phase measurements to reconstruct the absolute

trajectory of the chaser with a precision at the submeter level (Montenbruck et al., 2005). The resulting calibration errors are believed to be reduced to 0.1 mm/s.

3.2. Target Identification

Detecting reliably the target is not really a problem at mid and close-range, where the luminosity of the object allows for an unambiguous recognition of the target, but this becomes more challenging at far-range, where it is impossible to recognize at the first glance whether a luminous spot in the image represents a faint star, a hot pixel or a satellite. The use of a star catalog comes naturally in mind to help distinguishing the target from celestial objects. However, this approach is not sufficient to discriminate between all the objects present in the image, because some stars might not be included in the catalog or simply because additional non-stellar objects might be simultaneously visible.

As already stated, most of the time some additional *a priori* information is available by the means of TLEs. However, the poor accuracy of the TLEs makes them inappropriate for direct target recognition. At 10 km, a cross-track error of 500 m translates into about 3° error. Considering the typical field of view of the camera (18° x 14° in our case, cf. Table 2a), this results in a large search domain which could lead to numerous false detections. In view of measurement sparsity, it is however important to ensure that all the line-of-sight measurements refer to the same target, otherwise the additional outliers could prevent the convergence of the solution. The strategy retained in this work to ensure a robust and reliable target detection consists in associating a kinematic and a dynamic approach.

3.2.1. Kinematic Detection

The first step relies on the fact that, flying on a similar orbits, the apparent motion of the target seen by the chaser is very different from the motion of a star or from the motion of satellite flying on a different orbit. Imagine a camera pointing in the direction of flight, seeking for a satellite flying ahead (or behind) on almost the same orbit. Once the stars have been identified using a catalog, a few objects might remain unknown, so that additional intelligence is needed to select the desired target. As depicted in Fig. 8, when superimposing a sequence of images, some trajectories can be recognized, helping greatly the discrimination.

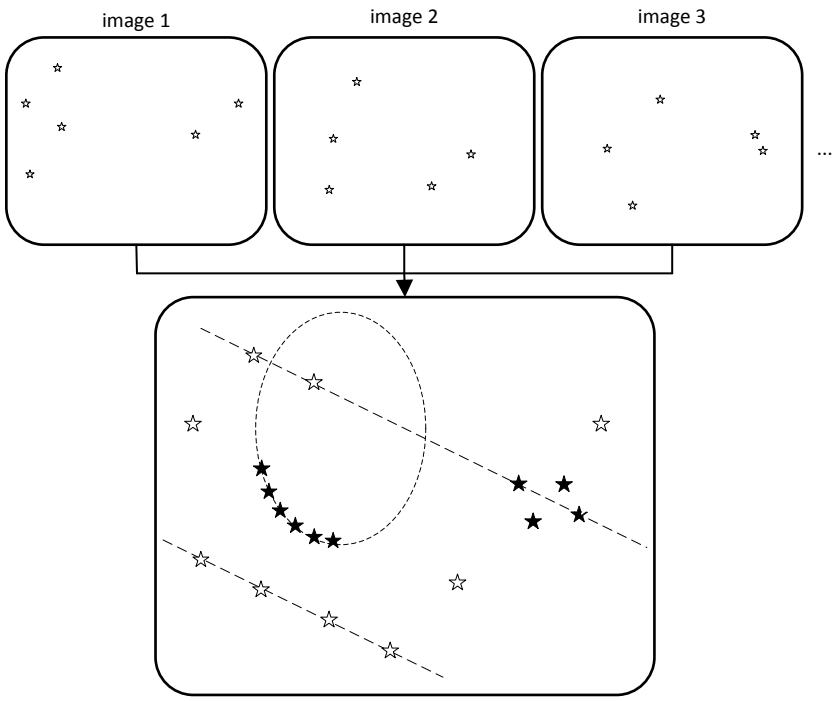

Figure 8: Density-based clustering of the non-recognized objects (the elliptical relative motion of the target is depicted by a dashed ellipse).

Of course, this is valid only if the camera is fixed in the local orbital frame, which might not be the case, if the orientation of the camera follows the target or in case of large attitude control errors. As a result, it is necessary to consider the history of the non-recognized objects as viewed by a virtual camera which is fixed in the local orbital frame. Afterward, the points belonging to the same trajectory are grouped using a clustering algorithm. The Density-Based Spatial Clustering of Applications with Noise (DBSCAN) (Ester et al., 1996) has been found extremely convenient for this purpose, since it allows grouping the points whose interdistance is below a certain threshold considering the other ones as noise. Since the distance traveled by the target object between two images is much smaller than the one of a non-recognized star or of a satellite flying on a different orbit, this clustering algorithm selects automatically the set of points which are likely to belong the same trajectory (black stars in Fig. 8).

DBSCAN requires only two parameters: the distance ϵ between the points

and the minimum number of points $n_{\min}$ required to form a dense region. Some care has to be taken for the definition of ϵ, which should correspond to the distance travelled by the satellite between two consecutive images, and which thus depends on the unknown target orbit. Several strategies are possible to set the value of ϵ:

- Based on simple considerations, set manually a coarse value able to capture a trajectory and reject the non-recognized stellar objects. Given the orbital period of the chaser satellite (about 90 minutes) and the time interval between two images (30 seconds), an inertially fixed celestial object would travel a distance of about 1.9° between two images which corresponds to about 80 pixels for the camera. Instead, a target object exhibiting a 2 km large elliptical relative motion (cf. Fig. 6) seen at 20 km would travel only 3-4 pixels between two images. As a result, a conservative value of $\epsilon = 10$ pixels should ensure the detection of the target (note that this is for the moment very similar to the detection based on the inertial angular velocity of the VBS sensor (Benn and Jørgensen, 2013), except that the orbital frame is used as reference frame to analyze the relative motion). However, it has to be emphasized that this approach is valid only if the coarse assumptions about the target relative motion are correct. In addition, the average distance travelled by the target between two images might vary a lot at mid and close-range, so that some adaptations of the threshold might be required throughout the complete approach.

- Since the orbit determination process requires anyway a reference target trajectory, the value of ϵ can also be derived from this guess relative orbit, based on the same considerations as before. In view of the figures derived above, a coarse value based on the size of the relative motion and the intersatellite distance should be enough (the exact apparent distance travelled between two images is the projection of a 3D elliptical motion on the focal plane of the camera and is tedious to compute). This is the solution which has been retained for this work, which computes a very coarse conservative value of ϵ based on the size of the relative elliptical motion in the RN plane (corresponding in a first approximation to the motion projected on the focal plane).

- A more elegant solution could be to derive the mean distance between the objects by analyzing the image without *a priori* information, as a

human eye would do. This would be useful for example for a survey of space debris or asteroids which could be discovered for the first time, but it however induces more complexity and is not really required in our case, since our target orbit is not unknown.

At this stage, DBSCAN has selected only clusters forming a dense region. In order to distinguish a trajectory (black cluster on the left in Fig. 8) from a conjunction of random non-recognized objects (right cluster in Fig. 8), the target identification algorithm relies on the fact that the relative motion of the spacecraft obeys to the space dynamics. The projection of its elliptic trajectory on the focal plane can thus be easily recognized as a curve. The algorithm attempts to identify this trajectory by fitting each cluster with a second order Bezier curve and by retaining the clusters which could be successfully fitted, based on the fitting residuals σ_{B}. The only limitation here is that a second-order Bezier curve can only describe a portion of trajectory, so that a sliding sequence of only 20 images (corresponding to 20 minutes) is used to recognize the trajectory piecewise. Considering typical centroiding errors of less than half a pixel and the fact that the Bezier curve is only an approximation of the real trajectory, the algorithm considers a fit as successful if $\sigma_{\mathrm{B}} < \sigma_{\mathrm{B,max}} = 1$ pixel. As depicted in Fig. 9, this simple strategy allows detecting trajectories among the clusters provided by the DBSCAN algorithm. The beauty of this approach is that, if the superimposition of images provides an apparent trajectory but the order of the points composing the trajectory is wrong (right case in Fig. 9), the algorithm will fail fitting a Bezier curve, since the parameter of the curve is chosen to be the time stamp of the images.

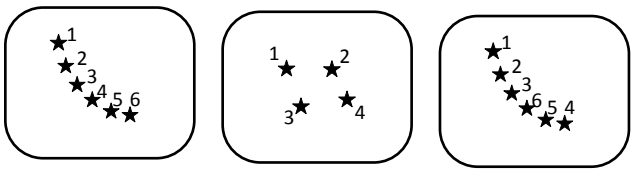

Figure 9: Bezier fits: success (left) and failures (middle and right).

This kinematic approach is appealing, since it requires little a priori knowledge about the orbit the target, but might however fail in some rare cases:

- if a hot pixel appears, an object would be recognized as being fixed in the orbital frame, which could in principle correspond to a satellite seen

at very large distance (a 500-meter-large relative elliptical orbit seen at 100 km would also be almost fixed) or a pure along-track (V-bar) approach. Similarly, if a conjunction of random nonrecognized objects appears with very small interdistance, a Bezier curve with $\sigma_{\mathrm{B}} < \sigma_{\mathrm{B,max}}$ could be found by fitting the cluster.

- if another satellite is visible on a similar orbit (for example, a spacecraft launched with the same rocket) several trajectories can be simultaneously visible.

As a consequence, in some cases the algorithm will find several possible plausible trajectories. In some other cases, it will provide a single wrong trajectory, if a parasite target is visible instead of the desired one. As result, an additional validation of the target detection has to be performed, before delivering the angles-only observations to the relative orbit determination process. This data screening is described in Section 3.2.4, but before addressing it, let us first formalize the ideas described above.

3.2.2. Algorithm Description

Fig. 10 depicts the different steps involved in the target detection. In the sequel, all objects imaged by the camera are considered as n point sources, whose centroids $\boldsymbol{p}_i$ have first to be determined. This task is a basic star tracker functionality and recalled here for completeness. In a first step, all pixels $\boldsymbol{c}$ whose intensity $I(\boldsymbol{c})$ is greater than the background noise σ_{c} are selected, forming a set $\mathcal{L}$ of luminous pixels which are distributed over the whole image:

$$\mathcal{L} = \{\boldsymbol{c} : I(\boldsymbol{c}) > \sigma_{\mathrm{c}}\} \tag{3}$$

The pixels referring to the same object have to be grouped in n clusters $\{\mathcal{O}_i\}$. For this purpose, several methods exist. The DBSCAN algorithm can be for simplicity advantageously recycled (for example with $\epsilon = 2$ and $n_{\min} = 2$, so that any group of more than 2 pixels will be considered as an object $\mathcal{O}$). Once the objects are formed, their centroiding can be computed using a simple arithmetic mean:

$$\boldsymbol{p}_i = \sum_{\boldsymbol{c}\in\mathcal{O}_i} I(\boldsymbol{c})\boldsymbol{p}_i \cdot \frac{1}{\sum_{\boldsymbol{c}\in\mathcal{O}_i} I(\boldsymbol{c})} = \sum_{\boldsymbol{c}\in\mathcal{O}_i} I(\boldsymbol{c})\boldsymbol{p}_i \cdot \frac{1}{s_i}, \tag{4}$$

where s_i can be taken as a measure of the brightness of the object. The pixel position $\boldsymbol{p}_i$ is then transformed in a line-of-sight measurement $\boldsymbol{u}_{\mathcal{C},i}$ (expressed

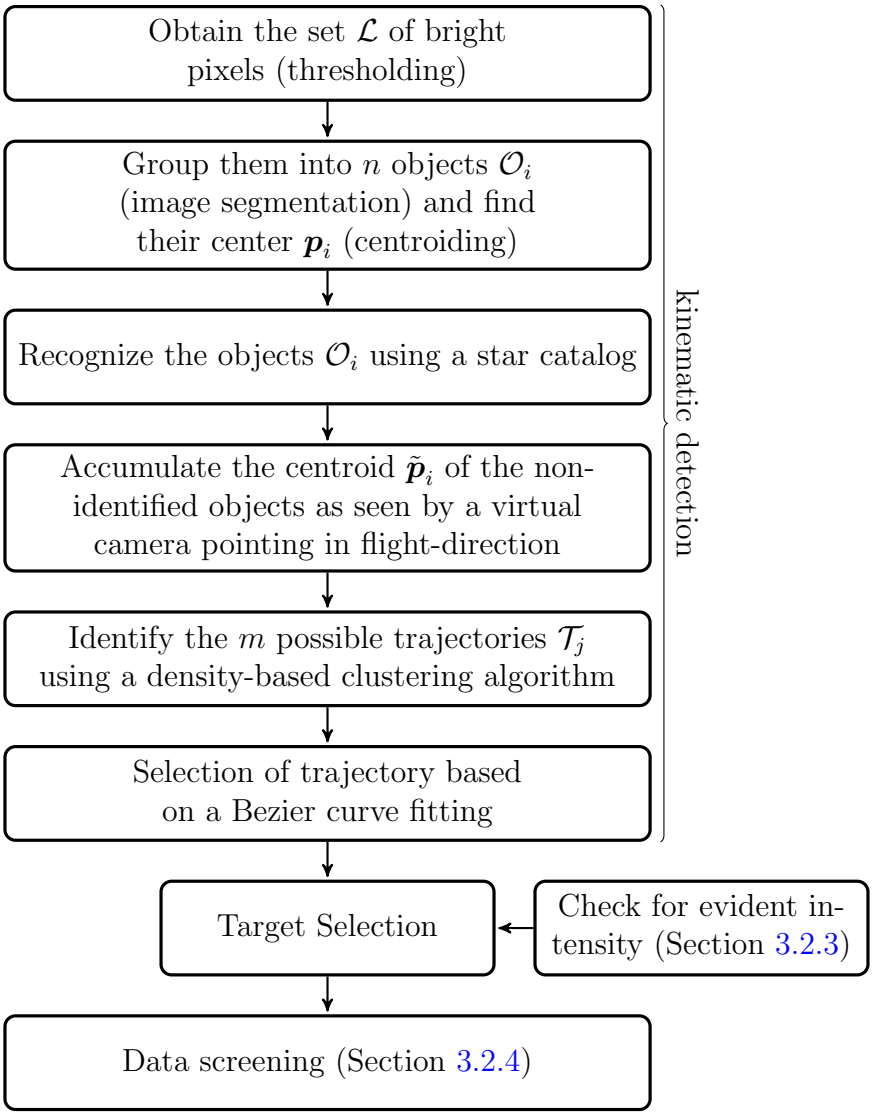

Figure 10: Functional view of the target detection algorithm.

in the camera frame $\mathcal{C}$) to the object $\mathcal{O}_i$ after taking the intrinsic camera parameters γ into account (comprising focal length, principal points, skew coefficient and distortion):

$$\boldsymbol{u}_{\mathcal{C},i} = \boldsymbol{g}^{-1}(\boldsymbol{p}_i, \gamma) \tag{5}$$

For our needs, a simplified camera model $\boldsymbol{g}$ (mapping a unit vector into a

pixel position) considering a pinhole camera accompanied with lens distortion has been found sufficient. This model is provided by Bouguet Bouguet (2004) and directly derived from the model proposed by Heikkila and Silven (Heikkila and Silven, 1997) . In this model, the pixel position $\boldsymbol{p}$ depends on the normalized position $\hat{\boldsymbol{p}}(\boldsymbol{u}) = \left(u_1/u_3, u_2/u_3\right)^T$:

$$\boldsymbol{p} = \begin{pmatrix} f_1 & 0 & \xi_1 \\ 0 & f_2 & \xi_2 \end{pmatrix} \begin{pmatrix} (1 + k\|\hat{\boldsymbol{p}}\|^2) \cdot \hat{\boldsymbol{p}} \\ 1 \end{pmatrix}, \tag{6}$$

where $\boldsymbol{f}$ is the focal length in pixels, the subscript i refers to the i^{th} component of a vector, $\boldsymbol{\xi}$ is the camera principal point coordinates in pixels and k the main radial distortion coefficient (note that no skew coefficient has been retained for simplicity).

The knowledge of the line-of-sight $\boldsymbol{u}_{\mathcal{C}}$ of the objects present in the image allows the identification of the celestial objects. This can be done either using a lost-in-space approach, in which the stars are identified without any *a priori* information, or using the onboard knowledge of spacecraft attitude together with the mounting information of the camera. Once the stars are identified, the extrinsic camera parameters (that is, the orientation of the camera $\boldsymbol{R}_{\mathcal{I}}^{\mathcal{C}}$ in the inertial frame $\mathcal{I}$) can be derived, for example using the q-method (Davenport, 1965).

At this stage, a set of still unidentified objects $\{\mathcal{O}_i\}$ remains. The next step is to recreate their virtual image $\tilde{\boldsymbol{p}}_i$ as seen in the frame $\mathcal{V}$ of a virtual camera perfectly pointing in the flight-direction:

$$\tilde{\boldsymbol{p}}_i = \boldsymbol{g}(\boldsymbol{R}_{\mathcal{I}}^{\mathcal{V}} \cdot \boldsymbol{R}_{\mathcal{C}}^{\mathcal{I}} \cdot \boldsymbol{g}^{-1}(\boldsymbol{p}_i, \gamma)), \tag{7}$$

It is time now to run the DBSCAN algorithm on the set of unrecognized objects $\tilde{\boldsymbol{p}}_i$. In order to reduce the number of possible candidates, it is at this stage advised to accumulate only those unrecognized objects which are compatible with the coarse information provided by the TLEs (in view of their poor accuracy, a large search area in the image might be selected but at least the remaining part is rejected). The output of the clustering algorithm is a set of m clusters $\{\mathcal{T}_j\}$ representing all possible trajectories. The next step is to try to fit the clusters $\{\mathcal{T}_j\}$ with a second order Bezier curve $\boldsymbol{B}(\tau)$, parameterized by the variable τ and defined by a set of three control points $\boldsymbol{\Xi}_0$, $\boldsymbol{\Xi}_1$ and $\boldsymbol{\Xi}_2$.

$$\boldsymbol{B}(\tau) = (1-\tau)^2\boldsymbol{\Xi}_0 + 2\tau\boldsymbol{\Xi}_1 + \tau^2\boldsymbol{\Xi}_2, \tau \in [0,1] \tag{8}$$

In view of the simple expression of the Bezier curve, fitting the data is trivial and can be done using a least-squares approach. Here the parameter τ has to capture the fact that the trajectory is a time-dependent suite of points. This can be achieved by considering the timestamp t_k of the points $\tilde{\boldsymbol{p}}_k$ composing a cluster $\mathcal{T}$. If $t_{\min}$ and $t_{\max}$ denote respectively the oldest and newest timestamp of the set of points composing $\mathcal{T}$, the parameter τ_k associated to the point $\tilde{\boldsymbol{p}}_k$ can be defined as

$$\tau_k = \frac{t_k - t_{\min}}{t_{\max} - t_{\min}} \tag{9}$$

so that the oldest point will be associated with $\tau = 0$ and the newest point with $\tau = 1$

3.2.3. Target Brightness

It certainly did not escape the notice of the Reader that, until now, the brightness of the target has never been used. This is due to the fact that, at far-range, the brightness information can hardly be used in a reliable way. In fact, the quantity of light reflected by the target spacecraft depends on its attitude which is unknown, since we are dealing with noncooperative targets. Fig. 11 depicts for instance the variation of brightness that has been observed during the ARGON experiment, when the spacecraft were separated by 28 km.

Figure 11: Variation of brightness during one orbit at 28 km (ARGON experiment).

At mid and close-range instead, the object becomes so bright that an obvious detection based on this criterion becomes possible. The measure s of brightness as defined in Eq. 4 can be used for this purpose. Here, some calibration is required to get an idea on the specific values obtained with a given sensor and the chosen exposure time. Fig. 12a depicts for instance the brightness of 10000 stars measured during the ARGON experiment and ordered according to their magnitude.

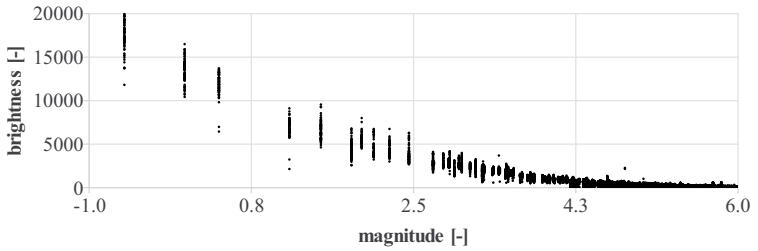

(a) Star brightness (exposure time = 0.5 s).

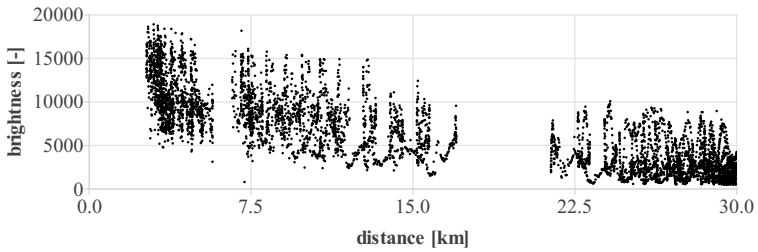

(b) Brightness of the Tango spacecraft during the approach.

Figure 12: Brightness measured using the μASC during the ARGON experiment.

The brightness of the target depends in addition on the object itself (size and surface) and will vary if the electronic shutter is used at mid to close-range. As a consequence, some care has to be taken while defining a brightness detection threshold. Fig. 12b depicts the luminosity of the target measured during the ARGON approach and shows that a detection threshold of $s = 5000$ would capture the few stars with magnitude below 2.5 (which are anyway included in any star catalog and can easily be recognized) and the target at a distance smaller than about 7 km. Note that the knowledge of the planets should be also available to avoid false detections, because they can be as bright as the most luminous stars. The advantage here is that this additional detection based on the brightness will work only at small separations, which corresponds exactly to the domain where the kinematic detection will experience a performance degradation, due to the increasing centroiding errors.

This latter effect can be better understood by looking at Fig. 13. The centroiding function will provide a measure of the center of the satellite based on the centroid of the flare which might differ greatly from the center of mass. Of course, at far-range this does not matter, since one pixel is larger than the size of the object, but at mid and close-range, this is not true anymore.

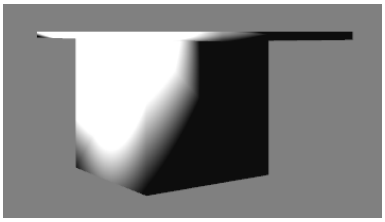

Figure 13: Example of unfavorable target illumination: the measured centroid will be far from the center of mass.

The kinematic detection tries to fit the target trajectory with a Bezier curve, which might fail in the presence of large centroiding errors. A detection based on the brightness can help mitigating this loss of performance.

3.2.4. Additional Data Screening

The kinematic detection might sporadically deliver wrong trajectories corresponding to parasite objects, which need to be filtered out before the least-squares adjustment. One might wonder why this additional data screening is required. Since the algorithm fails apparently only in rare occurrences, the healthy observations will greatly outnumber the misdetections so that, notwithstanding the few outliers, a proper estimate of the trajectory can be derived. This is of course correct in case of continuous observations like ARGON. But in the case of AVANTI, the problem is much more delicate. In this case, in view of the weak observability and sparse measurements, a few large outliers could prevent the convergence of the least-squares process. This is also due to the fact that a line-of-sight error of several degrees (corresponding to a wrong target detection in the search area delimited by the TLEs) is several orders of magnitude larger than the expected measurement noise and can thus quickly endanger the integrity of the least-square solution.

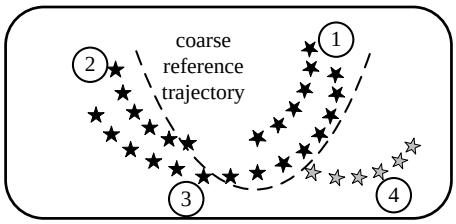

Figure 14: Statistical discriminations of wrong trajectories.

Several approaches could be implemented to mitigate this problem. One

possibility could consist in considering the entire collections of pieces of trajectories detected in the virtual frame and try to recognize the few trajectories which obviously do not belong to the same relative orbit based on the statistical distribution, as a human eye would do. This idea is depicted in Fig. 14: four pieces of trajectories have been found, but the gray one corresponds obviously to another spacecraft. This is of course easier said as done. A clustering algorithm could help treating this problem by grouping the observations which form a dense region and rejecting the outliers. However, this approach has been found by the Authors difficult to implement in a reliable way because the distance between the observations varies considerably during the entire approach, making difficult the formation of clusters. Further investigations are probably needed here to develop a more reliable clustering algorithm.

In view of the aforementioned difficulty, a simpler approach has been retained in this work, consisting in a basic data screening against the reference solution. The drawback of this strategy is that long data arcs are often needed to improve the observability. Starting from a reasonable guess reference trajectory, the pattern of line-of-sight errors is likely to grow exponentially when propagating over the complete data arc. Fig. 15 illustrates this phenomenon by depicting the line-of-sight errors between the measurements provided by the target detection and a reference solution using the flight data of the ARGON experiment. Even if the *a priori* solution is not bad at the beginning, small uncertainties regarding the initial conditions have a dramatic impact after several days. As a result, it might be difficult to automatically detect outliers based on simple thresholding. Here again, a clustering algorithm like DBSCAN is of great help to discard the isolated points which are too far from the main error pattern. The advantage of such an approach is shown in Fig. 15, where the gray crosses correspond to the measurements which have been rejected after analyzing the error pattern with DBSCAN.

3.3. Batch-Least Squares Adjustment

Provided that a set of line-of-sight measurements is available, the reconstruction of the relative orbit by the means of a least-squares adjustment is straightforward and recalled here for completeness. The relative trajectory is described in the form of a differential equation associated with an initial value $\boldsymbol{x}_0$ at time t_0:

$$\dot{\boldsymbol{x}} = \boldsymbol{f}(\boldsymbol{x}, t) \tag{10}$$

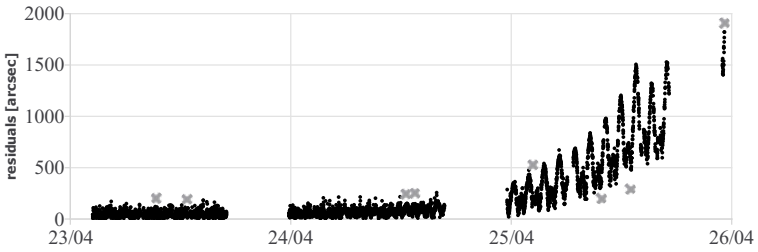

Figure 15: Line-of-sight errors over a long data arc starting from a coarse reference trajectory (ARGON experiment). The gray crosses correspond to outliers detected by the data screening.

$\boldsymbol{f}$ is a time-dependent function of a state vector $\boldsymbol{x}$ and describes the relative motion model. In low-Earth orbits, this model should at least include the perturbation due to the Earth-oblateness (J_2) and to the differential drag. The state vector $\boldsymbol{x}$ is composed of the inertial relative position $\boldsymbol{r}$ and relative velocity $\boldsymbol{v}$ of the target object with respect to the chaser. In order to estimate the relative drag as part of the orbit determination process, the state vector is augmented with the drag coefficient of the chaser spacecraft C_D:

$$\boldsymbol{x} = \begin{pmatrix} \boldsymbol{r} & \boldsymbol{v} & C_D \end{pmatrix} \tag{11}$$

In view of the weak observability of the problem and the sparse measurements, it has been chosen to restrict at maximum the number of estimated parameters. As a direct consequence, the maneuvers execution errors are for example not estimated. The unit vector $\boldsymbol{u}$ describing the line-of-sight from the chaser to the target spacecraft in the inertial frame $\mathcal{I}$ can be conveniently parameterized by a set of two angles (α,δ) named respectively right-ascension and declination:

$$\boldsymbol{u} = \frac{\boldsymbol{r}}{\|\boldsymbol{r}\|} = \begin{pmatrix} \cos(\alpha)\cos(\delta) \\ \sin(\alpha)\cos(\delta) \\ \sin(\delta) \end{pmatrix} \tag{12}$$

The line-of-sight measurement $\boldsymbol{u}$ is extracted from an image according to the algorithms described in Section 3.2.2 to build the pair of angular measurements:

$$\boldsymbol{h} = \begin{pmatrix} \alpha \\ \delta \end{pmatrix} = \begin{pmatrix} \arctan(\frac{u_2}{u_1}) \\ \arcsin(u_3) \end{pmatrix} \tag{13}$$

The least-squares adjustment requires the computation of the Jacobian ma-

trix, which can be derived using Eq. 12 and Eq. 13:

$$\boldsymbol{H} = \frac{\partial \boldsymbol{h}}{\partial \boldsymbol{x}_0} = \frac{\partial \boldsymbol{h}}{\partial \boldsymbol{r}} \frac{\partial \boldsymbol{r}}{\partial \boldsymbol{x}_0} = \begin{pmatrix} -\frac{r_2}{r_1^2+r_2^2} & \frac{1}{\frac{r_2^2}{r_1}+r_1} & 0 \\ -\frac{r_1 r_3}{r^2+\sqrt{1-\frac{r_3^2}{r}}} & -\frac{r_2 r_3}{r^2+\sqrt{1-\frac{r_3^2}{r}}} & \frac{\frac{1}{r}-\frac{r_3^2}{r^3}}{\sqrt{1-\frac{r_3^2}{r}}} \end{pmatrix} \frac{\partial \boldsymbol{r}}{\partial \boldsymbol{x}_0} \tag{14}$$

The derivation of the least-squares solution is well-known and is not recalled here for concision. A numerical integration is used to propagate the relative motion, using the dynamical model summarized in Table 1. The covariance matrix $\boldsymbol{P}$ is of great interest for us in the sequel. First because the introduction of the *a priori* $\boldsymbol{P}_0^{\text{apr}}$ covariance helps the convergence of least-squares solution in case of weak observability by constraining the search. Second, because the diagonal elements yield the standard deviation $\boldsymbol{\sigma}$ of the solution, which provides a measure of the achievable accuracy. In view of the strong anisotropy of the problem and in order to ease the following discussions, it is more convenient map this value in the Radial-Tangential-Normal frame and to restrict it to its first three components, corresponding to the relative position. As a result, the variable $\boldsymbol{\sigma}_{\text{r}}^{\text{RTN}}$ will be often used in the sequel as measure of achievable accuracy for $\boldsymbol{r}_0$.

Items	Value
Gravity model	JGM3 20x20
Atmospheric density model	Harris-Priester
Solar radiation pressure	applied
Luni solar perturbations	applied
Satellite area	cannonball model

Table 1: Relative motion model used for the propagation.

The design of the batch least-squares estimator relies on the provision of a reference trajectory derived from TLEs. In order to simplify the interfaces, it might be appealing to first try to compute a guess of the relative state using only line-of-sight measurements. This process, called angles-only Initial Relative Orbit Determination (IROD) in the literature, is not trivial and has attracted recently considerable attention. The major difficulty lies in the weak observability of the estimation problem. Woffinden (2008) demonstrated that, under the assumption of linear homogeneous relative dynamics, the problem is not observable in the Cartesian frame. Many authors have

proposed solutions to overcome this issue: using a second optical sensor at a known baseline, exploiting the camera offset with respect to the center of mass (Geller and Klein, 2014), formulating the problem using cylindrical coordinates (Geller and Lovell, 2017), or considering the nonlinearity (Garg and Sinclair, 2015) and the pertubations of the relative motion model. However, most of these solutions are not really applicable to the experimental conditions offered by AVANTI and ARGON. Either because they are valid for small (a few dozen meters) or large separations (more than 1000 km), or would require unattainable sensor performance (line-of-sight precision at the μrad level). In view of these limitations, an initialization based on TLEs has been preferred. Future work will investigate if some IROD methods may still be employed.

4. Flight Results

4.1. First Look at Far-Range

This analysis tackles the problem of approaching for the first time a non-cooperative object at far-range. In this scenario, it is assumed that a coarse orbit phasing has been already performed by the ground segment based on the available TLEs of the target. In view of the poor accuracy of the TLEs, no passive safety can be enforced at this stage, since the values of the relative eccentricity and inclination vectors cannot be determined accurately enough using TLEs. As a result, a safe separation of several dozen kilometers is kept during the orbit phasing.

The strategy here is to simply keep the camera pointing in flight direction, hoping that the target will become visible at some point. If the orbit phasing has been done correctly, the large separation ensures that the apparent relative motion is entirely contained in the field of view of the camera. At this safe distance, the longitudinal direction is difficult to estimate accurately, since only large and costly maneuvers would induce a perceptible change of relative motion. But this matters little. It is in fact much more judicious to exploit the complementarity between the TLEs and the line-of-sight measurements, in order to focus on the motion perpendicular to the flight direction (i.e. in the RN plane). The power of this strategy can be demonstrated using a simple example from the ARGON experiment. Let us observe the Tango satellite on 23 April 2012 during only two orbits (between 18:00 and 21:00), when the spacecraft are separated by 30 km. The orbits are chosen to be maneuver-free, making the problem very weakly observable. Let us now

consider that we have few clues about the target orbit, assuming thus a pure along-track separation of 25 km. In view of the weak observability and the limited observation time, the least-squares adjustment is likely to diverge. If we now constrain the problem by introducing the *a priori* covariance $\boldsymbol{P}_0^{\text{apr}}$ corresponding to the accuracy of a coarse orbit phasing based on TLEs (errors of 5 km for the position and 50 m/s for the velocity), the process is able to converge to provide an estimate $\boldsymbol{x}_0$ at epoch t_0=2012/4/23 18:00:00.

A priori	$a\delta\boldsymbol{\alpha}_0^{\text{apr}} = \begin{pmatrix} 0 & 0 & 0 & 0 & 0 & -25000 \end{pmatrix}$m
Estimated	$a\delta\boldsymbol{\alpha}_0 = \begin{pmatrix} -2 & -83 & -417 & 1 & 246 & -33500 \end{pmatrix}$ m
Reference	$a\delta\boldsymbol{\alpha}_0^{\text{ref}} = \begin{pmatrix} -6 & -80 & -370 & 3 & 220 & -30000 \end{pmatrix}$m

(a) Orbit determination results.

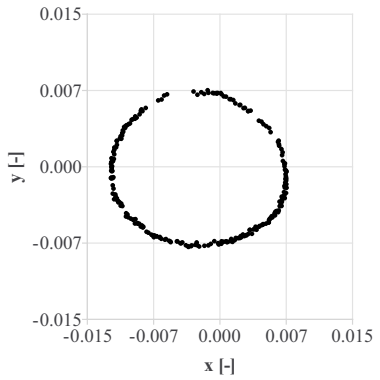

(b) Normalized coordinates $\hat{\boldsymbol{p}}$ of the target measured in the virtual frame $\mathcal{V}$.

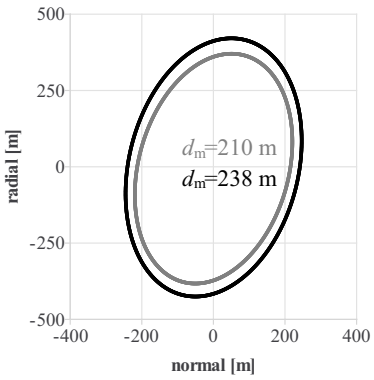

(c) Estimated (black) vs. true (gray) relative motion in the RN plane.

Figure 16: Relative orbit determination with a priori covariance at far-range (ARGON).

Table 16a summarizes the orbit determination results (the state vectors are expressed in terms of dimensional relative orbital elements $a\delta\boldsymbol{\alpha}$ for simplicity and the drag coefficient is omitted). The reference relative state is derived from the GPS-based relative orbit determination products. It can be observed that, without the need of executing any maneuver, the relative orbit determination is already able to estimate $a\delta a$ accurately to a few meters. This is of great importance, since $a\delta a$ drives directly the rhythm of the rendezvous, so that its accurate knowledge ensures a smooth approach. As far as the passive safety is concern, the error of the estimated vectors $a\delta\boldsymbol{e}$ and $a\delta\boldsymbol{i}$ amount to about 10% of their size, allowing establishing already at

that stage passively safe orbits. Figure 16c depicts graphically the estimated and the true relative motion in the RN plane, showing that the shape of the orbit has been properly reconstituted but its size has been overestimated by about 10% (simply because the distance has been as well overestimated by 10%), leading to a slightly too optimistic minimum distance $d_{\min}$. Let us redo the same exercise using the data collected during AVANTI, by selecting a 4-hour-long data arc on 24 September 2016, when the spacecraft are separated by 45.6 km (according to TLEs).

A priori	$\delta\boldsymbol{\alpha}_0^{\text{apr}} = \begin{pmatrix} 0 & 0 & 0 & 0 & 0 & 45000 \end{pmatrix} m$
Estimated	$\delta\boldsymbol{\alpha}_0 = \begin{pmatrix} -30 & -534 & 670 & 4 & 852 & 48500 \end{pmatrix} m$

(a) Orbit determination results.

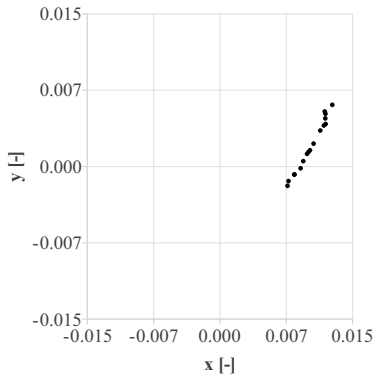

(b) Normalized coordinates $\hat{\boldsymbol{p}}$ of the target measured in the virtual frame $\mathcal{V}$

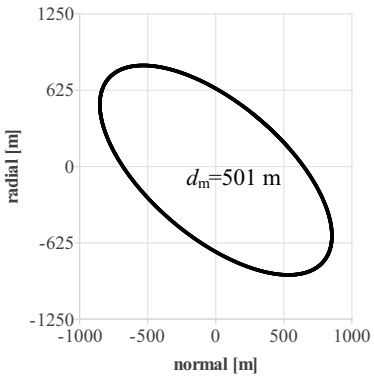

(c) Estimated relative motion in the RN plane.

Figure 17: Relative orbit determination with a priori covariance at far-range (AVANTI).

Here again, the relative orbit determination is aided by the same covariance matrix $\boldsymbol{P}_0^{\text{apr}}$ and the a priori reference trajectory assume a pure along-track separation of 45 km. As shown in Fig. 17b, the visible relative motion is dramatically reduced. Here again, there is no chance to perform a successful orbit determination without constraining the problem. But the interesting outcome is that, despite the tiny portion of observations, it is also possible to estimate the shape of the relative motion at this distance and establish a passively safe relative orbit. In the absence of external reference, it is of course difficult to assess the quality of this estimation. One interesting comparison consists in estimating the relative motion this time without any *a*

priori covariance information. The main problem for this exercise is that, in order to improve greatly the observability and enable the convergence of the least-squares filter, one would need to alter considerably the relative motion, which is usually not the preferred approach. In order to keep a reasonable propellant budget, an alternative strategy consists in executing small maneuvers and observing the resulting effect over a longer time interval. This idea was retained in AVANTI, where a single 1.2 cm/s maneuver has been executed on 23 September. Small maneuvers will only improve slightly the observability, requiring thus a longer observation arc (typically several days) to ensure the convergence of the least-squares process. However this comes at the cost of a degradation of the dynamical model over the considered arc, because the mismodeling errors will become predominant. To illustrate this idea, two orbit determinations have been done with different data arcs lengths (5 and 7 days).

Table 2: Orbit determination without a priori covariance with different data arcs.

Data arc	2016/9/21 - 2016/9/26	2016/9/21 - 2016/9/28
Observations	346	444
Residuals (α, δ)	$0 \pm 33'', 0 \pm 35''$	$0 \pm 38'', 0 \pm 42''$
$a\delta\boldsymbol{\alpha}_0$	$\begin{pmatrix} 4 & -724 & 555 & 2 & 875 & 47227 \end{pmatrix}$ m	$\begin{pmatrix} 13 & -860 & 691 & 2 & 1041 & 57261 \end{pmatrix}$ m
C_D	2.39	1.91
Standard deviation $\boldsymbol{\sigma}_\mathrm{r}^\mathrm{RTN}$	$\begin{pmatrix} 164 & 7269 & 133 \end{pmatrix}$ m	$\begin{pmatrix} 101 & 4205 & 76 \end{pmatrix}$ m

The results are summarized in Table 2 and are not especially consistent. This example has been chosen to highlight the difficulty to choose the proper length of the data arc. By selecting 5 days of observations, the standard deviation of the least-squares solution indicates a large uncertainty in the along-track direction (7 km). Is is thus tempting to increase the data arc in order to reduce the standard deviation, but then the data fitting degrades.

A close look on the residuals pattern in Fig. 18 can help assessing the quality of the orbit determination. The residuals of 30" correspond to measurement noise of less than half a pixel (one pixel is equivalent to 80"). Some data gaps can be observed : they corresponds to time intervals where the chaser had to interrupt the observation due to thermal problems on the BIROS satellite. A closer look in Fig. 18b shows that the residuals of the 7-day solution (especially of the declination) slightly increase and cannot be considered as white noise anymore, indicating that the quality of the orbit determination is probably not as good as the one done with the 5-day-long arc,

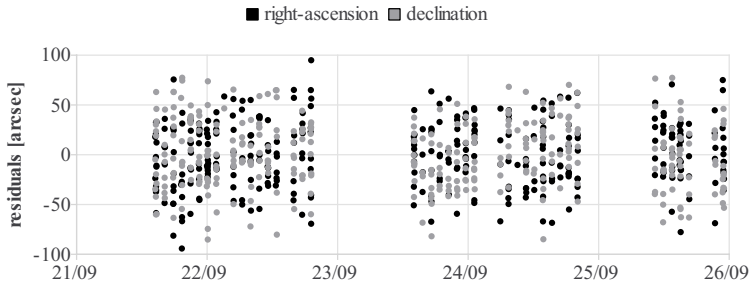

(a) 5 days.

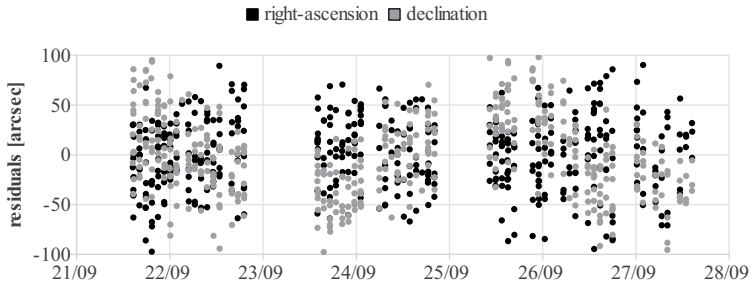

(b) 7 days.

Figure 18: Relative orbit determination without a priori covariance at far-range (AVANTI).

because the dynamical model is not adapted anymore. At far-range, some dexterity is thus required to select the best compromise between observability and validity of the dynamical model, as well as to judge the quality of the products. These are however subtle considerations, since the accuracy of the relative orbit determination will anyway improve with decreasing distance and since, despite the difficulty in estimating properly the range, the different orbit determinations provide already a very good estimate of the shape of the relative motion. Figure 19 depicts for instance the difference between the relative motion in the RN plane estimated using orbit determinations performed with and without a priori covariance . As expected after the quick quality analysis of the residuals, the 5-day solution shows a good match with the solution computed using the a priori covariance.

4.2. Far to Mid-Range Approach

As soon as larger variations of the apparent relative motion can be observed, the difficulties described in the previous section disappear. The orbit

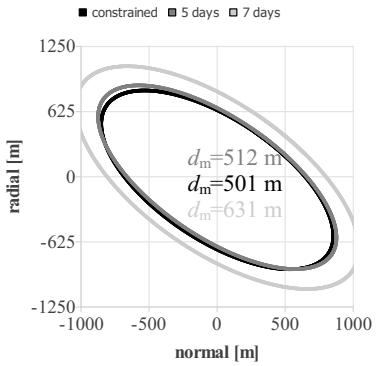

Figure 19: Estimated relative motion in the RN plane on 24 September 2016 12:00 using orbit determinations with (black) and without (dark and light gray) a priori covariance (AVANTI).

determination becomes able to converge rapidly and consistent results are observed between consecutive data arcs. Here again, the skill of the user is required to select the more appropriate length for the data arc, long enough to ensure observability and short enough to minimize the impact of the errors of the relative motion model. As usual, let us refresh our mind with the almost perfect experimental conditions offered by the ARGON experiment. For this purpose, the pictures collected with the PRISMA satellites have been reprocessed over a 4-day-long data arc.

Figure 20 depicts the variation of distance during ARGON and the line-of-sight residuals after least-squares adjustment. At close distance, the target becomes so bright that the stars in the background are not visible anymore. This problem will be described more in details in the next section. For the moment, it has been decided to simply reject all the images if less than 6 stars are visible (since in this case, no precise estimation of the orientation of the camera can be done). This explains why the number of observations decreases when approaching. In view of the rapid change of relative motion (from 30 km to 3 km over 5 days), the problem is well observable, so that excellent accuracy can be achieved. Figure 21 depicts the orbit determination errors (with respect to the GPS-based relative positioning products), at the meter level for all the components except for $a\delta\lambda$ which exhibits an error up to a few hundred meters (consistently with the results formerly obtained during ARGON (D'Amico et al., 2013)).

It appears now interesting to focus on the remaining error sources. Obvi-

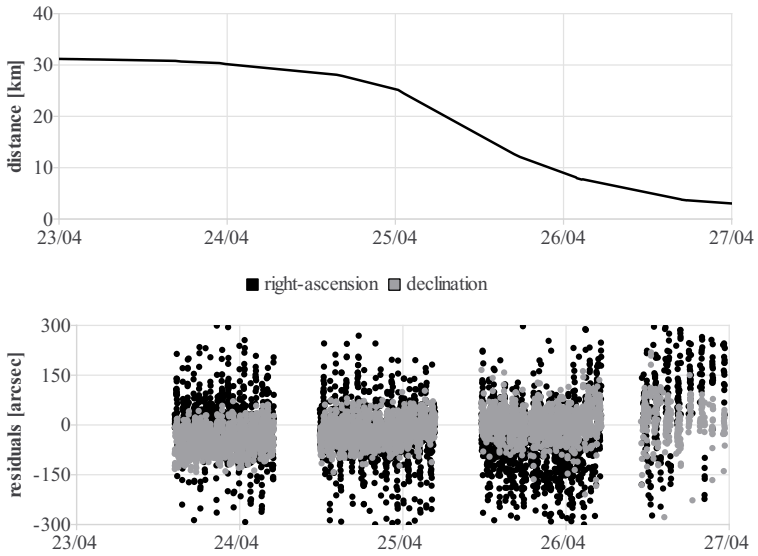

Figure 20: Intersatellite distance and residuals during the ARGON experiment (2012).

ously, the systematic centroiding errors due to the truncation of information in the Regions of Interests (as documented in (D'Amico et al., 2013)) plays a role in the overall error budget. The second obvious source of errors lies in the relative motion model, and in particular in the errors due to the maneuvers. The fact that the least-squares process considers the entire data arc constitutes at the same time its force (to improve the observability) and its weakness, since the mismodelling are summed up over the complete arc. During the 4-day-long data arc, 26 maneuvers have been executed, with as many maneuver execution errors which are introduced in the relative motion model. Since the PRISMA satellites were fully cooperative, it is tempting *a posteriori* to recalibrate the maneuvers using differential GPS (Allende-Alba et al., 2017), to investigate the influence of maneuver execution errors. The least-squares solution obtained with the fine calibration of the maneuvers is depicted for comparison in Fig. 21. A clear improvement can be seen. Note that this is a pure academic exercise, since in reality it is impossible to calibrate maneuvers using differential GPS with a noncooperative target. Once the error due the maneuvers is well reduced, the remaining perturbation of the relative motion model is mainly due to the differential drag. It can be seen that the filter is not really able to capture the time variation of $a\delta a$, accumulating an error of about 3 m in 4 days, resulting in a error of a few

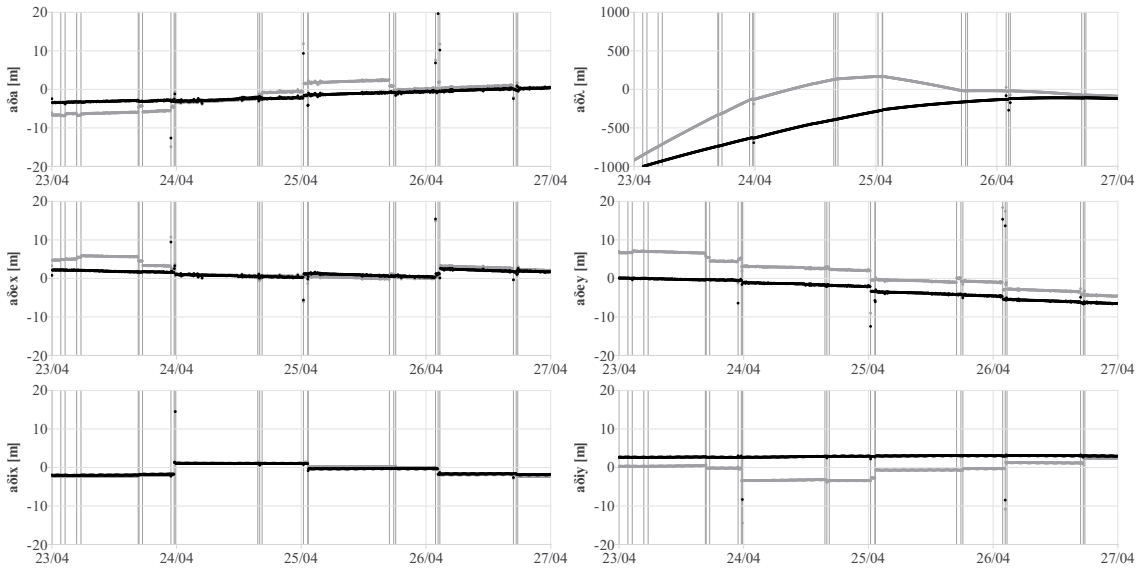

Figure 21: Error of the estimated relative orbital elements for both angles-only orbit determinations, using coarse (gray) and fine (black) maneuver calibration. The maneuvers are represented by gray vertical lines (ARGON).

hundreds meters in $a\delta\lambda$. The orbit determination results using both fine and coarse maneuver calibration are summarized in Table 3.

Table 3: Relative orbit determination result using coarse (gray) and fine (black) maneuver calibration (ARGON).

Maneuver	coarse calibration	fine calibration
Data arc	2012/4/23 - 2012/4/27	2012/4/23 - 2012/4/27
Observations	4461	4499
Residuals (α, δ)	$19 \pm 90'', 11 \pm 49''$	$17 \pm 90'', 17 \pm 45''$
$a\delta\boldsymbol{\alpha}_0$	$\begin{pmatrix}-7 & -83 & -390 & -4 & 202 & -30038\end{pmatrix}$	$\begin{pmatrix}-3 & -85 & -397 & -3 & 204 & -31151\end{pmatrix}$
C_D	3.85	3.78
$\boldsymbol{\sigma}_\mathrm{r}^\mathrm{RTN}$	$\begin{pmatrix}0.2 & 27.8 & 0.1\end{pmatrix}$	$\begin{pmatrix}0.2 & 27.4 & 0.1\end{pmatrix}$

For AVANTI, these difficulties are exacerbated by the fact that considerably less measurements are available and that the perturbation of the differential drag is much stronger. In addition, this perturbation is far from being constant. In the current design of the relative orbit determination facility, a constant value for the drag coefficient C_D is estimated over the whole data

arc. In reality, the constraints posed by the satellite during AVANTI results in frequent changes of attitude profiles to satisfy the mission requirements, inducing large variations of the cross-sectional area of the chaser. Fig. 22 depicts for example the area subject to the differential drag in different attitude modes: Earth-pointing (in order to orient the communication antennas to the ground), Target-pointing (when tracking the target with the star tracker), and cool-down mode (when the spacecraft needs to be actively cooled).

(a) Earth-pointing (b) Target-pointing (c) Cool-down

Figure 22: Variation of cross-sectional area for different attitude profiles (AVANTI).

These difficulties have to be kept in mind but, luckily, do not prevent us from completing our task. Fig. 23 depicts for instance more than one month of relative orbit determination, covering a large part of the commissioning phase as well as the first autonomous approach (19 to 23 November). The gray zones correspond to different arcs for the relative orbit determination. The 154 maneuvers executed during this period have not been represented for clarity. Note at the boundaries how accurately the different solutions match with respect to each other. Small discrepancies can be sometimes recognized (for example between the first and second data arc for $a\delta a$) but the errors remained limited to a few percent. In fact, only a closer look to the standard deviation of the solution (last plot in Fig. 23) can provide us with a better insight into the achieved accuracy of the solution.

A clear correlation between the intersatellite distance and the performance of the orbit determination can be recognized. Starting with a pretty large along-track error of about 1 km at 40 km (cf. previous section), the accuracy improves when the distance between the satellites decreases, reaching relative positioning performance at the meter level when the separation drops below 1 km (for example on 16 November). This feature belongs to the magic part of angles-only navigation: the relative navigation accuracy improves when it is needed. The estimated drag coefficient C_{D} of the chaser spacecraft is also represented for each orbit determination arc (gray lines in the upper plot

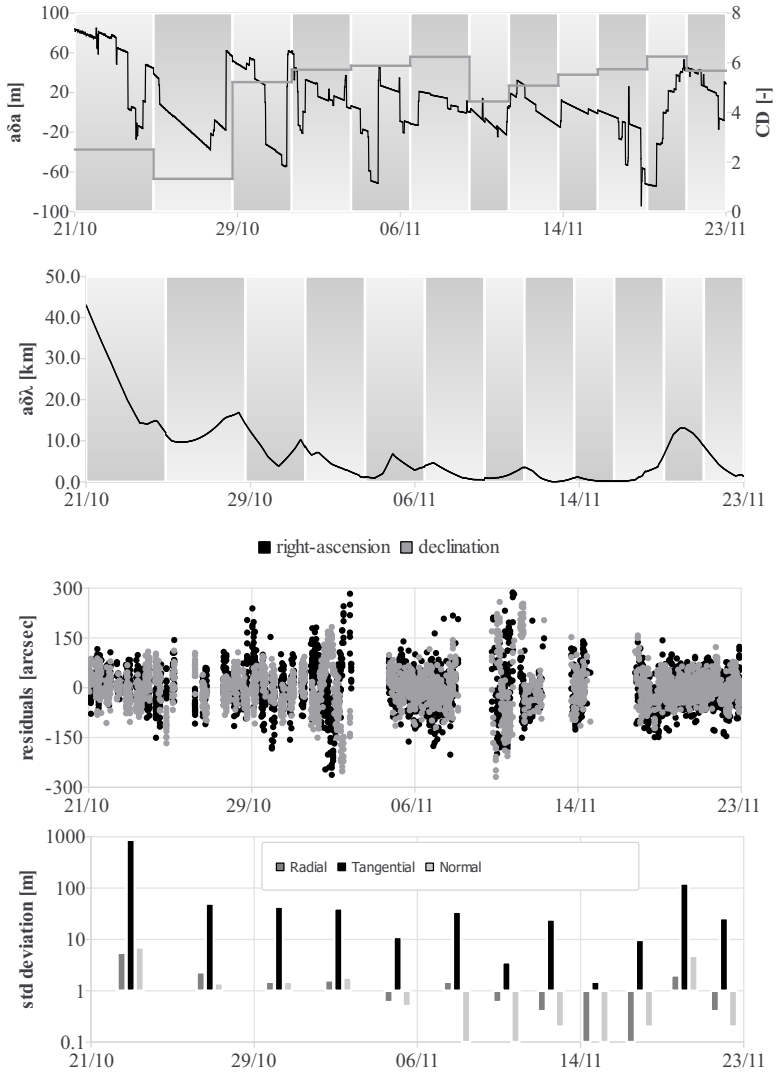

Figure 23: One month of relative orbit determination during the AVANTI campaign.

of Fig. 23 associated to the right y-axis). Obviously, unrealistic values are obtained. They correspond to the fact that the orbit determination tends to capture the mean effect of the differential drag over the whole arc. Further improvements are probably needed to better model this perturbation (it can also be that the adopted model of the atmospheric drag (Harris-Priester) is too inaccurate).

As far as the image processing is concerned, it seems that the assumptions

done in Section. 3.2 were fully justified. Fig. 24 shows the Bezier curve fitting residuals and measured brightness for the tracked objects. In both experiments, the fitting residuals are pretty similar, indicating that the centroiding performance is almost the same for Tango and BEESAT-4. The chosen limit $\sigma_{\mathrm{B,max}} = 1$ pixel seems to be adequate for the whole approach. The brightness is instead fairly different, which was expected considering the difference of size (10x10 cm against 30x30 cm). It can been observed that the intensity of Tango is limited. This is due to the fact that an automatic electronic shutter had been used during ARGON, while this functionality was not yet activated during the considered data arc for AVANTI (cf. next section).

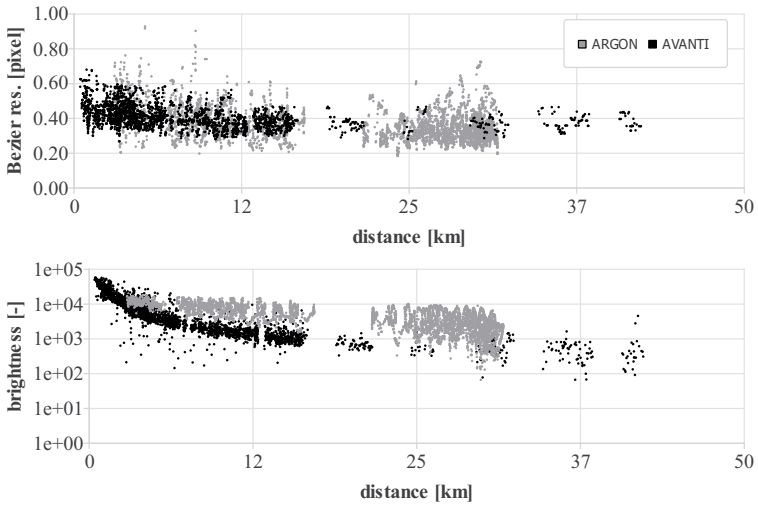

Figure 24: Output of the image processing for both experiments.

In the absence of other external reference, the discussions about the navigation performance are based on the analysis of the covariance of the solution, which provides a measure of the achievable orbit determination accuracy but, practically, this measure "is often found to be too optimistic in the presence of systematic force and measurement model error" (Montenbruck and Gill, 2001). This statement is easily illustrated by the discrepancies observed for ARGON between the orbit determination errors (Fig. 21), which indicates a lateral and longitudinal accuracy at the meter and hectometer level, while the standard deviation (Table 3) pretends to reach a performance at the submeter and decameter level. Still, this does not mean that this value cannot be exploited, rather that it has to be considered with care. In order to assess the validity of the assumptions used for relative orbit determination, a radar

campaign has been conducted as independent means of verification using the German TIRA system. The radar on ground suffers however from the difficulty to discriminate the signals reflected by the chaser and target satellites if the intersatellite distance is too small. Consequently, it has been decided to conduct this campaign when the satellites were far away (more than 40 km distance). Three radar passes have been scheduled on 20-21 October, following the recommendations of the in-house expertise already available in this domain (Kahle et al., 2014). The resulting radar-based orbit determination is expected to be affected by an error of about 2 m in the radial direction and 20 m in the other directions (Kahle et al., 2014). For the angles-only orbit determination, a data arc spanning 5 days (18 to 22 October) has been selected for relative orbit determination, where a controlled approach had been initiated from ground to bring the formation back to 15 km separation.

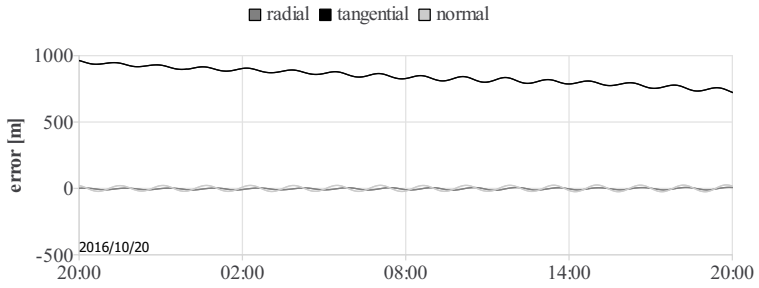

Figure 25: Orbit determination errors: angles-only vs. radar-based solution (AVANTI).

Fig. 25 depicts the relative orbit determination errors compared to the radar-based solution in the local orbital frame. As expected at this distance, the longitudinal error is much larger (two orders of magnitude) than the lateral error. Looking at the covariance of the solution, the relative orbit determination claims to be accurate to [5.5 873.8 7.3] m in the RTN frame, which is perfectly consistent with the observed errors, giving thus confidence that assumptions retained for relative orbit determination were correct.

A close look to the relative orbit elements gives more weight to what has already been emphasized: at this distance, what counts is to control smoothly the drift rate of the approach and to establish a safe relative orbit, not really to know exactly the intersatellite separation (which is in our case anyway estimated accurately to 2%). Fig. 26 shows that, already at this distance, the relative semi-major axis is estimated accurately at the meter level. Its decay due to the differential drag is as well estimated pretty decently.

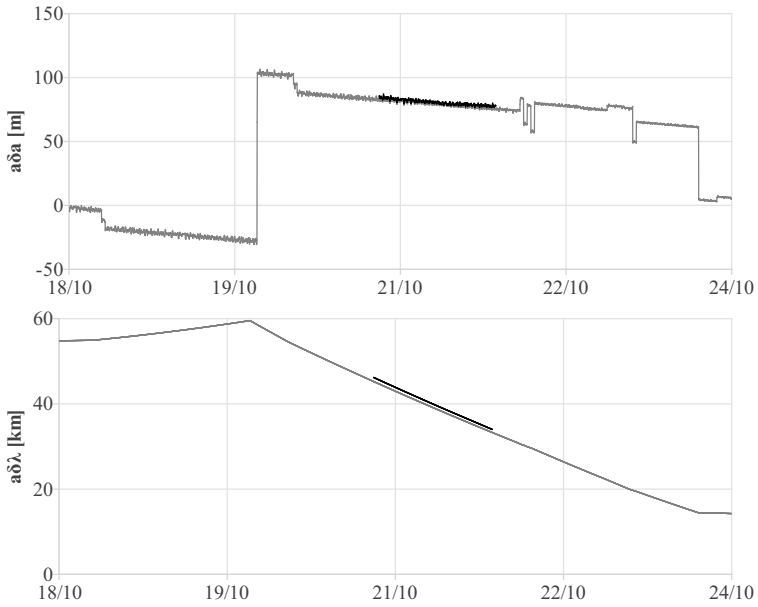

Figure 26: Angles-only vs. radar-based solutions (AVANTI).

As already mentioned, the covariance information should be handled with care, since it does not always faithfully reflect the actual error of the solution. However, it has to be emphasized that the lateral relative orbit determination performance is more important from an operational point of view (in order to assess the risk of collision). The concept of passive safety offered by the spiraling approach requires indeed a good knowledge of the Radial-Normal components of the relative motion. The risk of collision becomes relevant at mid-to-close range, where the lateral performance predicted by the covariance is at the submeter level while the true error can amount to several meters. As a result, some safety margin (typically 10 m) should be applied when monitoring the minimum intersatellite distance d_m in the plane perpendicular to the flight direction (cf. Section 2.4). Future work will focus on more detailed covariance analysis, trying to understand the contribution of the different error sources (maneuver execution errors, improper drag modeling, measurement bias) and aiming at building a more realistic covariance, able to serve as reliable measure for the error of the solution.

4.3. Towards Close-Range...

Angles-only navigation comes naturally in mind to support far-to-mid range rendezvous. In this case, the target spacecraft is imaged as a point whose centroid matches accurately the actual center of mass, and the stars visible in the background ensure a precise knowledge of the orientation of the camera. All these aspects contribute to provide line-of-sight measurements accurate at the subpixel level and allow for accurate relative orbit determination throughout the entire rendezvous.

In view of the satisfying performance obtained during the far-to-mid range approach, it was tempting to also investigate what would happen at closer distance. Can angles-only navigation also be used to bridge the mid-range gap, that is, to bring the target in the working range of close-proximity sensors?

The major difficulty during a close approach lies in the increasing brightness of the spacecraft, making mandatory the regulation of the exposure time. However, when reducing the exposure, the stars in background are not visible anymore and it becomes impossible to derive precisely the orientation of the camera. Another important limitation is due to the image of the target itself, which cannot be considered anymore as a point aligned with the center of mass (cf. Fig. 13). These two sources of error contribute greatly to degrade the accuracy of the line-of-sight measurements. But since the problem depends very much on the distance, these uncertainties are still acceptable for small separations. In fact, one degree measurement error corresponds to less than 1 m error at 50 m distance but translates into 174 m error at 10 km.

Two close approaches have been exercised during AVANTI, the first one (11-18 November, cf. Fig. 23) with a strong support from the ground as part of the commissioning phase, the second one fully autonomously. This section will only focus on the fully autonomous approach (24 to 27 November). The upper subplot of Fig. 27 depicts the estimated instantaneous intersatellite distance (not the mean along-track separation $a\delta\lambda$ anymore) during the approach. In the mid-subplot, the residuals in black refer to angles-only observations which have been derived using the stars in the background to estimate the orientation of the camera. The residuals in gray are instead computed when the onboard estimate of the attitude of the camera is used. For clarity, both right-ascension and declination measurements are merged with the same color.

When the electronic shutter is used, it becomes necessary to make use of the onboard attitude to compute the inertial line-of-sight observations. In

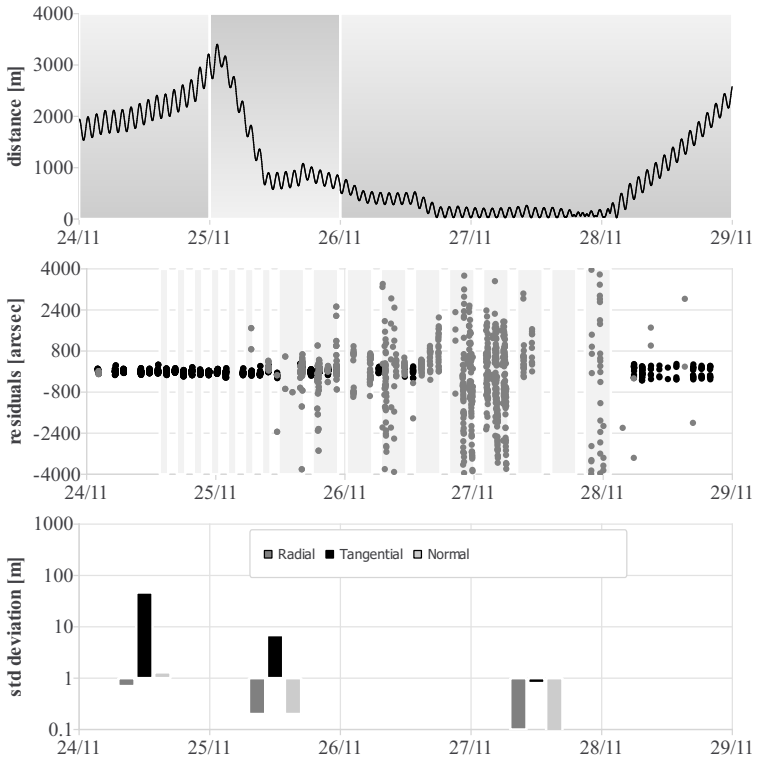

Figure 27: Orbit determination results during the close approach (AVANTI).

the case of AVANTI, since one of the star cameras was used to follow the target, it was unfortunately not possible to always keep a camera head pointed to the deep sky, so that the onboard attitude was sometimes affected by errors up to one degree! In view of this performance degradation, two different strategies have been investigated during the close approach. During some orbits, the sharpness of the target image has been sacrificed (by deactivating the electronic shutter) to obtain a more accurate line-of-sight observation thanks to a better attitude knowledge of the camera (for AVANTI this strategy is also helped by the limited and symmetrical shape of the target: the center of the bright blob is likely to be close to the center of mass). During the rest of the time, the electronic shutter was activated (depicted by gray areas in the residuals plot of Fig. 27), yielding accurate images but inaccurate angles-only observations. Fig. 28 shows the resulting target image at decreasing distance. Starting from an unrecognizable blob, specific features can be detected (rectangular shape and presence of two antennas).

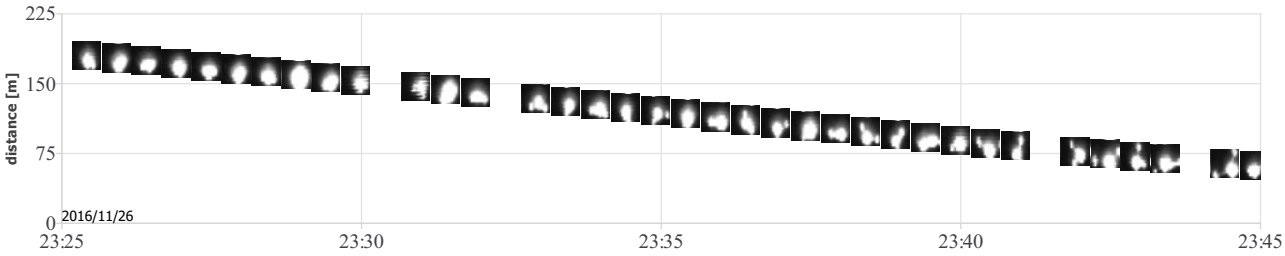

Figure 28: BEESAT-4 imaged a close range: coarse spacecraft features become observable at about 100 m (AVANTI).

Some adaptation of the measurement noise in the least-squares process is of course needed when including the observations derived with the coarse onboard attitude. During AVANTI, two different values (80" and 3600") were used depending on the presence of stars in the background. Note that the poor performance of the onboard attitude encountered during AVANTI is rather specific to the minimalistic design of the experiment (Gaias et al., 2017). If additional star trackers are available to measure precisely the spacecraft attitude, the reconstructed orientation of the camera is much more precise. Fig. 29 depicts for instance the line-of-sight residuals obtained with ARGON, already depicted in Fig. 20, but this time complemented with observations derived from the onboard attitude. The errors are clearly much smaller.

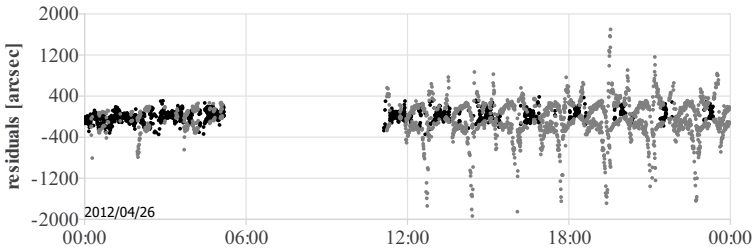

Figure 29: line-of-sight errors using the stars (black) and onboard attitude (gray) to estimate the orientation of the camera (ARGON).

Anyway, with this settings a precise reconstruction of the relative trajectory becomes possible even with degraded observations. According to the covariance of the solution, relative positioning accuracy at the sub-meter level is achieved at close range! In view of the discussions done before, the

real accuracy should be however probably at the meter level.

5. Conclusion

During more than two months, angles-only relative orbit determination has been continuously performed to support the AVANTI experiment, covering intersatellite separations from 50 km to 50 m. The resulting experience collected in orbit remarkably complements the legacy left by the precursor ARGON experiment, constituting thus a valuable collection of flight data and expertise. Despite the fact that both in-orbit demonstrations have been conducted in low Earth orbit and used the same camera to track the target object, substantial differences in terms of visibility and performance could be observed. These disparities are principally due to the choice of the orbit: while the ARGON experiment benefited from the optimal visibility conditions offered by a dawn-dusk configuration, AVANTI had to cope with eclipses and camera blinding, dramatically reducing the amount of observations. In addition, flying at lower altitude, AVANTI had to face much stronger orbital perturbations due to the differential drag. The design of the chaser impacts also considerably the flight results: ARGON could rely on the ideal experimental conditions offered by a dedicated formation-flying testbed, whereas AVANTI had to cope with numerous additional constraints. The complementarity of both experiments is anyway of great interest: ARGON presents easier navigation conditions but also the luxury of offering a precise reference based on differential GPS for performance validation. AVANTI explores instead the limits in terms of angles-only navigation and demonstrates that relative trajectory reconstruction can still be successfully performed under these conditions.

One of the difficulties in processing real data consists in reliably extracting the line-of-sight observations from the images. In fact, in view of the sparsity of the measurements encountered during AVANTI, a few outliers could endanger the integrity of the relative orbit determination. In order to tackle this problem, a dedicated target detection algorithm has been implemented, based on the kinematic recognition of relative trajectories. The best performance is obtained at far- to mid-range. At close-range the increasing centroiding errors might degrade the trajectory recognition but this issue can be easily mitigated by simply detecting the target based on its brightness. Additional data screening relying on a guess reference trajectory is finally performed to remove the possible outliers. Some room for improvement ex-

ists here in trying to execute this task without any *a priori* information, in order to make the target detection independent from the availability of TLEs. This aspect will probably be tackled in future investigations.

In view of the poor visibility and the strong orbit perturbations encountered during AVANTI, a batch least-squares approach has been preferred to ensure the robustness of the solution. In order to reduce the errors of the dynamical model, the maneuvers executed during the rendezvous are calibrated beforehand using the GPS data of the chaser spacecraft. Still the uncertainties of the differential drag model constitute a real-challenge for the orbit determination task. The current design adjusts the chaser drag coefficient to capture the effect of the differential drag over the considered data arc. This approach is however not fully satisfying, since a large part of the fluctuations of the differential drag is due to the peculiar attitude profile of the chaser. A refinement of the drag model based on the attitude of the chaser might help improving the orbit determination process and will be addressed in future work.

Overall angles-only navigation has been found to be a powerful method to approach a noncooperative target. AVANTI demonstrated that even a tiny picosatellite can be visible at a distance up to 50 km. At far-range, angles-only relative orbit determination exhibits large along-track errors up a few hundred meters but is already able to estimate accurately the shape of the elliptical relative motion, enabling thus already at this stage a smooth and safe rendezvous. The weak observability at very large separations (several dozen kilometers) might however prevent the convergence of the solution. In this case, constraining the least-squares solution around the relative orbit derived from TLEs is sufficient to mitigate this problem. Here again, further research focusing on initial orbit determination would be of benefit for the relative trajectory reconstruction, avoiding thus the need to seek assistance from TLEs. At mid-range and in the presence of large variations of the relative motion, this latter difficulty disappears, so that the relative trajectory could be successfully determined during all the approaches exercised during the AVANTI experiment. The achievable accuracy is shown to improve continuously throughout the entire rendezvous, promising relative navigation performance at the meter level at close-range according to the covariance of the solution.

Acknowledgments

The construction of the BIROS satellite was funded by the Federal Ministry of Education and Research of Germany (BMBF) (project number FKZ 01LK0904A).

References

, Jul. 2007. DARPA archive: Orbital express on-orbit mission updates. http://archive.darpa.mil/orbitalexpress/mission_updates.html, DARPA Tactical Technology Office, [retrieved 4 August 2017].

Allende-Alba, G., Montenbruck, O., Ardaens, J.-S., Wermuth, M., Hugentobler, U., 2017. Estimating maneuvers for precise relative orbit determination using GPS. Advances in Space Research 59 (1), 45 – 62, doi:10.1016/j.asr.2016.08.039.

Ardaens, J.-S., D'Amico, S., Montenbruck, O., 2011. Final Commissioning of the PRISMA GPS Navigation System. 22st International Symposium on Spaceflight Dynamics, Brazilian Institute for Space Research, São José dos Campos, Brazil.

Baumann, F., Trowitzsch, S., Brieß, K., 2012. BEESAT - A CubeSat Series Demonstrates Novel Picosatellite Technologies. 4th European CubeSat Symposium, Brussels, Belgium.

Benn, M., Jørgensen, J. L., 2013. Autonomous Vision Based Detection of Non-stellar Objects Flying in Formation with Camera Point of View. In: Proceedings of the 5th International Conference on Spacecraft Formation Flying Missions & Technologies (SFFMT). DLR, German Space Operations Center, Munich, Germany.

Benninghoff, H., Tzschichholz, T., Boge, T., Gaias, G., 2013. A Far Range Image Processing Method for Autonomous Tracking of an Uncooperative Target. 12th Symposium on Advanced Space Technologies in Robotics and Automation, Noordwjik, The Netherlands.

Bodin, P., Noteborn, R., Larsson, R., Karlsson, T., D'Amico, S., Ardaens, J.-S., Delpech, M., Berges, J.-C., 2012. PRISMA Formation Flying Demonstrator: Overview and Conclusions from the Nominal Mission. No. 12-072.

35th Annual AAS Guidance and Control Conference, Breckenridge, Colorado, USA.

Bouguet, J.-Y., 2004. Camera Calibration Toolbox for Matlab. http://www.vision.caltech.edu/bouguetj/calib_doc/ [Accessed 1 September 2017].

Chari, R. J. V., 2001. Autonomous Orbital Rendezvous Using Angles-Only Navigation. Ph.D. thesis, Massachusetts Institute of Technology. Dept. of Aeronautics and Astronautics., U.S.A.

Cropp, A., 2001. Pose estimation and relative orbit determination of a nearby target microsatellite using passive imagery. Ph.D. thesis, University of Surrey, U.K.

D'Amico, S., Ardaens, J.-S., Gaias, G., Benninghoff, H., Schlepp, B., Jørgensen, J. L., 2013. Noncooperative Rendezvous Using Angles-Only Optical Navigation: System Design and Flight Results. Journal of Guidance, Control, and Dynamics 36 (6), 1576–1595, doi: 10.2514/1.59236.

D'Amico, S., Gill, E., Garcia, M. F., Montenbruck, O., 2006. Gps-based real-time navigation for the prisma formation flying mission. 3rd ESA Workshop on Satellite Navigation User Equipment Technologies, NAVITEC, Noordwijk, The Netherlands.

Davenport, P. B., Nov. 1965. A Vector Approach to the Algebra of Rotations with Applications. NASA x-546-65-437, NASA.

Delpech, M., Berges, J.-C., Djalal, S., Christy, J., 2012. Vision Based Rendezvous Experiment performed during the PRISMA Extended Mission. In: Proceedings of the 23rd International Symposium on Space Flight Dynamics. Jet Propulsion Laboratory, Pasadena, California, USA.

Ester, M., Kriegel, H.-P., Sander, J., Xu, X., 1996. A Density-Based Algorithm for Discovering Clusters in Large Spatial Databases with Noise. In: Proceedings of the 2nd International Conference on Knowledge Discovery and Data mining. p. 226–231.

Fehse, W., 2003. Automated Rendezvous and Docking of Spacecraft. Cambridge University Press.

Gaias, G., Ardaens, J.-S., 2016. Design challenges and safety concept for the avanti experiment. Acta Astronautica 123, 409–419, doi: 10.1016/j.actaastro.2015.12.034.

Gaias, G., Ardaens, J.-S., Schultz, C., 2017. The AVANTI experiment: flight results. In: Proceedings of the 10$^{\text{th}}$ International ESA Conference on Guidance, Navigation & Control Systems. European Space Agency, ESTEC, Noordwijk, The Netherlands.

Gaias, G., Ardaens, J.-S., Terzibaschian, T., 2015. Paving the Way for Future On-Orbit-Servicing Missions: the AVANTI Experiment. In: Proceedings of the 25$^{\text{th}}$ International Symposium on Space Flight Dynamics ISSFD. DLR, German Space Operations Center, Munich, Germany.

Gaias, G., D'Amico, S., Ardaens, J.-S., 2014. Angles-Only Navigation to a Noncooperative Satellite Using Relative Orbital Elements. Journal of Guidance, Control, and Dynamics 37 (2), 439–451, doi: 10.2514/1.61494.

Garg, S., Sinclair, A., 2015. Initial Relative-Orbit Determination Using Second-Order Dynamics and Line-of-Sight Measurements. 25$^{\text{th}}$ AAS/AIAA Space Flight Mechanics Meeting, Williamsburg, Virginia.

Geller, D. K., Klein, I., 2014. Angles-only navigation state observability during orbital proximity operations. Journal of Guidance, Control, and Dynamics 37 (6), 1976–1983, doi: 10.2514/1.G000133.

Geller, D. K., Lovell, T. A., 9 2017. Angles-Only Initial Relative Orbit Determination Performance Analysis using Cylindrical Coordinates. The Journal of the Astronautical Sciences 64 (1), 72–96.

Grzymisch, J., Fichter, W., 2015. Optimal Rendezvous Guidance with Enhanced Bearings-Only Observability. Journal of Guidance, Control, and Dynamics 38 (6), 1131–1140, doi: 10.2514/1.G000822.

Halle, W., Bärwald, W., Terzibaschian, T., Schlicker, M., Westerdorf, K., 2014. The DLR -Satellite BIROS in the Fire-Bird Mission. In: Proceedings of the 4S Symposium: Small Satellites, Systems and Services. 26 - 30 May 2014, Majorca, Spain, European Space Agency, Noordwijk, The Netherlands.

Hammel, S. E., Aidala, V. J., 1985. Observability Requirements for Three-Dimensional Tracking via Angle Measurements. IEEE Transactions on Aerospace and Electronic Systems 21 (2), 200–207.

Heikkila, J., Silven, O., 1997. A four-step camera calibration procedure with implicit image correction. In: Proceedings of the 1997 Conference on Computer Vision and Pattern Recognition (CVPR '97). CVPR '97. IEEE Computer Society, Washington, DC, USA.

Jørgensen, J., Benn, M., 2010. Vbs - the optical rendezvous and docking sensor for prisma. NordicSpace, 16–19.

Jørgensen, J., Denver, T., Betto, M., Jørgensen, P., Röser, H.-P., Sandau, R., Valenzuela, A., 2003. The micro asc, a miniature star tracker. Small Satellites for Earth Observation, 4th International Symposium of the International Academy of Astronautics, pp. 157–162.

Kahle, R., Weigel, M., Kirschner, M., Spiridonova, S., Kahr, E., Letsch, K., 2014. Relative Navigation to Non-cooperative Targets in LEO: Achievable Accuracy from Radar Tracking Measurements. Int. J. Space Science and Engineering 2 (1), 81–95.

Montenbruck, O., Gill, E., 2001. Satellite Orbits - Models, Methods, and Applications. Springer Verlag.

Montenbruck, O., Kirschner, M., D'Amico, S., Bettadpur, S., 2006. E/I-Vector Separation for Safe Switching of the GRACE Formation. Aerospace Science and Technology 10 (7), 628–635, doi: 10.1016/j.ast.2006.04.001.

Montenbruck, O., van Helleputte, T., Kroes, R., Gill, E., 2005. Reduced Dynamic Orbit Determination using GPS Code and Carrier Measurements. Aerospace Science and Technology 9 (3), 261–271.

Nardone, S. C., Aidala, V. J., 1981. Observability Criteria for Bearings-Only Target Motion Analysis. IEEE Transactions on Aerospace and Electronic Systems 17 (2), 162–166.

Nardone, S. C., Graham, M. L., 1997. A closed-form solution to bearings-only target motion analysis. IEEE Journal of Oceanic Engineering 22 (1), 168–178.

Noteborn, R., Bodin, P., Larsson, R., Chasset, C., 2011. Flight Results from the PRISMA Optical Line of Sight Based Autonomous Rendezvous Experiment. In: Proceedings of the 4th International Conference on Spacecraft Formation Flying Missions & Technologies (SFFMT). Canadian Space Agency, St-Hubert, Quebec.

Persson, S., Jakobsson, B., Gill, E., 2005. PRISMA - Demonstration Mission for Advanced Rendezvous and Formation Flying Technologies and Sensors. No. 05-B56B07. 56th International Astronautical Congress, Fukuoka, Japan.

Roemer, S., Stoltz, S., 2010. SPL – Light Weight Deployment Mechanism for Single CubeSats and DPL for Double CubeSats. Symposium on Small Satellite Systems and Services (4S), Funchal, Madeira, Portugal.

Sabol, C., Vallado, D., 1999. A fresh look at angles-only orbit determination. No. AAS/AIA Vol. AAS 99-363. AAS/AIAA Astrodynamics Specialist Conference, Girdwood, Alaska.

Sullivan, F., D'Amico, S., 2017. Adaptive Filtering for Maneuver-Free Angles-Only Navigation in Eccentric Orbits. 27th AAS/AIAA Space Flight Mechanics Meeting, San Antonio, Texas.

Woffinden, D. C., 2008. Angles-Only Navigation for Autonomous Orbital Rendezvous. Ph.D. thesis, Utah State University, U.S.A.

Woffinden, D. C., Geller, D. K., 2009. Observability Criteria for Angles-Only Navigation. IEEE Transactions on Aerospace and Electronic Systems 45 (3), 1194–1208.

Yim, J. R., Crassidis, J. L., Junkins, J. L., 2004. Autonomous Orbit Navigation of Two Spacecraft System Using Relative Line of Sight Vector Measurements. No. 04-257. 14th AAS/AIAA Space Flight Mechanics Meeting, Maui, Hawaii.